

**NHC-GOLD(I) AND (III) COMPLEXES FOR USE IN ENERGY STORAGE
AND ARYL HALOGENATION**

by

Michael Ghidui

A thesis submitted to the Faculty of the University of Delaware in partial fulfillment of the requirements for the degree of Honors Degree in Chemistry with Distinction

Spring 2012

© 2012 Michael Ghidui
All Rights Reserved

**NHC-GOLD(I) AND (III) COMPLEXES FOR USE IN ENERGY STORAGE
AND ARYL HALOGENATION**

by

Michael Ghidui

Approved: _____
Joel Rosenthal, Ph.D.
Professor in charge of thesis on behalf of the Advisory Committee

Approved: _____
Susan Groh, Ph.D.
Committee member from the Department of Chemistry and Biochemistry

Approved: _____
Sherry Kitto, Ph.D.
Committee member from the Board of Senior Thesis Readers

Approved: _____
Michael Arnold, Ph.D.
Director, University Honors Program

ACKNOWLEDGMENTS

I would like to thank Dr. Joel Rosenthal for being a supportive mentor and helping to foster the development of my skills as a researcher. I would also like to thank Allen Pistner for his frequent help with setting up and running experiments. Dr. Glenn Yap solved the crystal structures reported in this thesis, and Dr. Steve Bai provided help with NMR experiments. Finally, I would like to thank the Rosenthal group, the staff at the Undergraduate Research program, my thesis committee for taking the time and effort to make this experience possible, and my friends and family for continued support.

This research was funded by the UD Science and Engineering Scholars Program, a Plastino Alumni Undergraduate Research Fellowship and 2011 Fall and 2012 Spring UD Undergraduate Research Supply and Expense Grants.

TABLE OF CONTENTS

LIST OF FIGURES	vi
ABSTRACT	viii
1 INTRODUCTION	1
1.1 Motivation for Alternative Energy Systems	1
1.2 Attractiveness of Solar Energy	2
1.3 Transition Metal Complexes in Solar Energy Conversion	4
1.4 Gold in Catalysis and Photochemistry	5
2 SYNTHESIS AND CHARACTERIZATION OF NHC-GOLD(I)/(III) CHLORIDE COMPLEXES FOR ENERGY STORAGE	7
2.1 Introduction	7
2.2 Results and Discussion	8
2.2.1 NHC-Gold Chloride Complexes	8
2.3 Conclusions	10
2.4 Experimental	10
2.4.1 General Considerations	10
2.4.2 Synthesis of NHC-Gold Chloride Complexes	11
2.4.3 Synthesis of NHC-Gold(III) HCl Complexes	11
2.4.4 Photochemical Studies	12
3 SYNTHESIS AND CHARACTERIZATION OF NHC-GOLD(I)/(III) ARYL COMPLEXES	13
3.1 Introduction	13
3.2 Results and Discussion	14
3.2.1 Phenyl Derivatives	14
3.2.2 Fluorinated Phenyl Derivatives	17
3.3 Conclusions	25
3.4 Future Work	26
3.5 Experimental	27

3.5.1	General Considerations	27
3.5.2	Synthesis of NHC-Arylgold Complexes	28
3.5.3	Photochemical Studies.....	32
3.5.4	Catalytic Studies.....	32
3.5.5	X-Ray Structure Determination.....	33
	REFERENCES.....	34

LIST OF FIGURES

Figure 1.1: Historical trends in electricity generation.	2
Figure 1.2: Methods of storing solar energy, compared by plotting power density against energy density.	3
Figure 1.1: Photocatalytic splitting of HX to form H ₂ and X ₂	5
Figure 2.1: Proposed photochemical cycle of NHC-gold(I) and (III) couples. The gold(I) complex (1) is oxidized <i>via</i> PhICl ₂ to the gold(III) complex (2), which then undergoes photoreductive elimination to reform the starting material.	7
Figure 2.2: UV-Vis time-course spectra for the photochemical reduction of AuCl ₃ (IPr) to AuCl(IPr) in dichloromethane (1.0 cm cuvette) over 2 hours.	9
Figure 2.3: ¹ H NMR time-course photoreduction of AuCl ₃ (IPr) to AuCl(IPr) over 2 hours. 400 MHz, CDCl ₃	9
Figure 3.1: Arylgold(I) complexes studied: AuPh(IPr) (3), AuC ₆ H ₄ F(IPr) (4), AuC ₆ H ₂ F ₃ (IPr) (5), AuC ₆ HF ₄ (IPr) (6), and AuC ₆ F ₅ (IPr) (7).	13
Figure 3.2: Photoreductive halogen elimination from bis-NHC-Au bromide complexes (R = Bn).	14
Figure 3.3: Tentative scheme for thermal reductive elimination of AuPh(IPr). The Au(I) complex is oxidized to form the Au(III) complex, which is unstable and quickly undergoes reductive elimination to form AuCl(IPr) and chlorobenzene.	15
Figure 3.4: ¹³ C NMR of AuPh(IPr) reductive elimination. Two spectra are overlaid; one of the reaction mixture (red) and one of authentic chlorobenzene (blue).	16
Figure 3.5: The molecular structures of AuC ₆ F ₅ Cl ₂ (IPr) (top) and AuC ₆ F ₅ (IPr) (bottom), with ellipsoids depicted at the 30% probability level. H atoms have been omitted for clarity.	18

Figure 3.6: ^1H NMR spectra of $\text{AuC}_6\text{F}(\text{IPr})$ after oxidation with PhICl_2 under two different conditions. The spectra have been truncated to show the characteristic isopropyl H septet. CDCl_3 , 400 MHz.	19
Figure 3.7: ^1H NMR spectra of $\text{AuC}_6\text{H}_2\text{F}_3(\text{IPr})$ after oxidation under two different conditions. The spectra have been truncated to show the characteristic isopropyl H septet. CDCl_3 , 400 MHz.	21
Figure 3.8: ^1H NMR spectra of $\text{AuC}_6\text{HF}_4(\text{IPr})$ after oxidation under various conditions. The spectra have been truncated to show the characteristic isopropyl H septet. CDCl_3 , 400 MHz.	22
Figure 3.9: UV-Vis time-course photoreduction over 20 hours for $\text{AuC}_6\text{F}_5\text{Cl}_2(\text{IPr})$. Spectra were taken every hour.	23
Figure 3.10: ^1H NMR time-course photoreduction for $\text{AuC}_6\text{F}_5\text{Cl}_2(\text{IPr})$ over 21 hrs, truncated to show the characteristic isopropyl H septet. All integrals were normalized to a 1,4-dioxane internal standard ($\delta = 3.7$). CDCl_3 , 400 MHz.	24
Figure 3.11: Reductive elimination in alkylgold(III) fluoride complexes.	27

ABSTRACT

N-Heterocyclic Carbene (NHC) complexes of gold(I) and gold(III) of the form AuX(IPr) and AuXCl₂(IPr) (IPr = 1,3-bis(2,6-diisopropylphenyl)imidazol-2-ylidene, X = halide or aryl) were prepared and investigated for photochemical activity. Where X = Cl, it was found that an energetically downhill oxidative addition could add an equivalent of Cl₂ which could then be subsequently photoreductively eliminated in an energetically uphill step, representing a model energy storage-and-release scheme for chemical fuel formation. Where X = aryl (fluorinated phenyl derivatives), oxidative addition of Cl₂ and subsequent reductive elimination produced the gold(I) complex AuCl(IPr) and the chlorinated aryl ligand. The reaction pathway was strongly dependent upon the electronics of the aryl ligand; more electron-rich ligands (X = phenyl) preferentially underwent thermal reductive elimination, while electron-poor ligands (X = pentafluorophenyl) could only be actuated photochemically. A gradient between these extremes was observed in intermediate ligands (X = 4-fluorophenyl, 2,4,6-trifluorophenyl, and 2,3,5,6-tetrafluorophenyl).

Chapter 1

INTRODUCTION

1.1 Motivation for Alternative Energy Systems

We are facing the reality that anthropogenic carbon emissions are causing atmospheric carbon dioxide (CO₂) concentrations to rise to unprecedented levels.¹ These levels are now nearing 400 ppm, up 80 ppm since 1960.² These levels are expected to increase in the future.¹ Carbon dioxide is a greenhouse gas, which traps excess heat radiated from Earth's surface, resulting in a rise of the average global temperature; this effect has been understood as early as 1896.³ Even small changes in this average temperature could have disastrous implications for world and local climate, such as dangerous irregularities in hydrological cycles and problems with flooding and erosion.^{4,5} Compounding this problem, there is also a steadily increasing global demand for energy that is expected to continue well into the future; this energy typically comes from relatively-inexpensive fossil fuels such as oil and coal, which are major contributors to greenhouse gas emissions (Figure 1.1).^{1,6,7} Global energy requirements in 2001 were estimated at 13.5 TW; by 2050 this is projected to increase to 27.6 TW, and 43.0 TW by 2100.⁸ In order to mitigate these problems, there is an imperative to develop new energy schemes that are not carbon-intensive to help satisfy this demand.

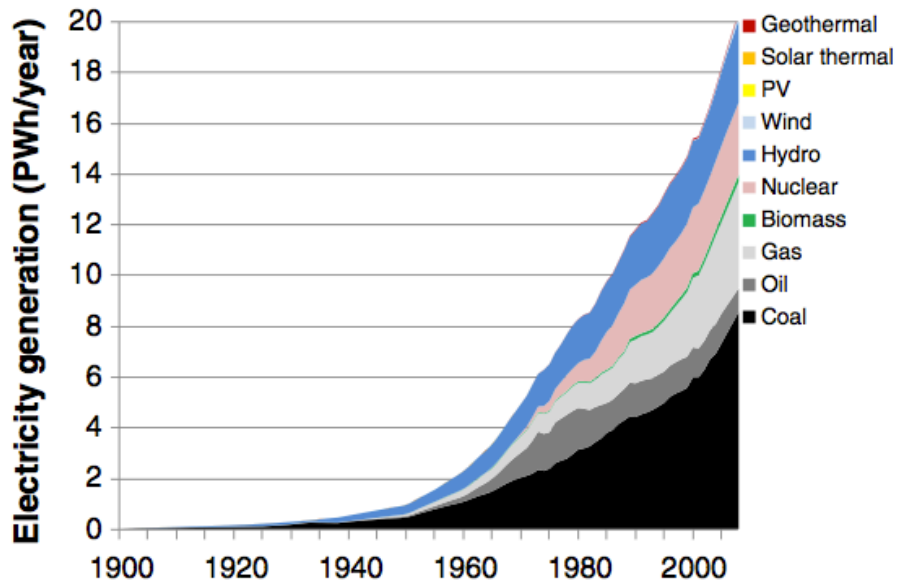


Figure 1.1: Historical trends in electricity generation.

1.2 Attractiveness of Solar Energy

Various avenues of alternative and renewable energy generation have been compared, including solar, wind, and nuclear power; of these, solar energy is the most attractive source for meeting the world's projected energy needs.^{9,10} At an annual power of 100,000 TW, the solar energy that strikes the Earth is plentiful enough to supply all of mankind's energy needs.¹¹ Solar energy can also be easily decentralized, meaning that energy is used close to its generation source as opposed to a grid distribution system; this makes it possible to cater to individual energy users and to be able to extend the technology to most of the people on the planet.⁹ However, solar energy is intermittent due to limited daylight and atmospheric effects. In order to become a viable energy source, the problem of energy storage will have to be solved

so that 24-hour utilization is possible. Figure 1.2 shows various methods for storing solar energy.⁹

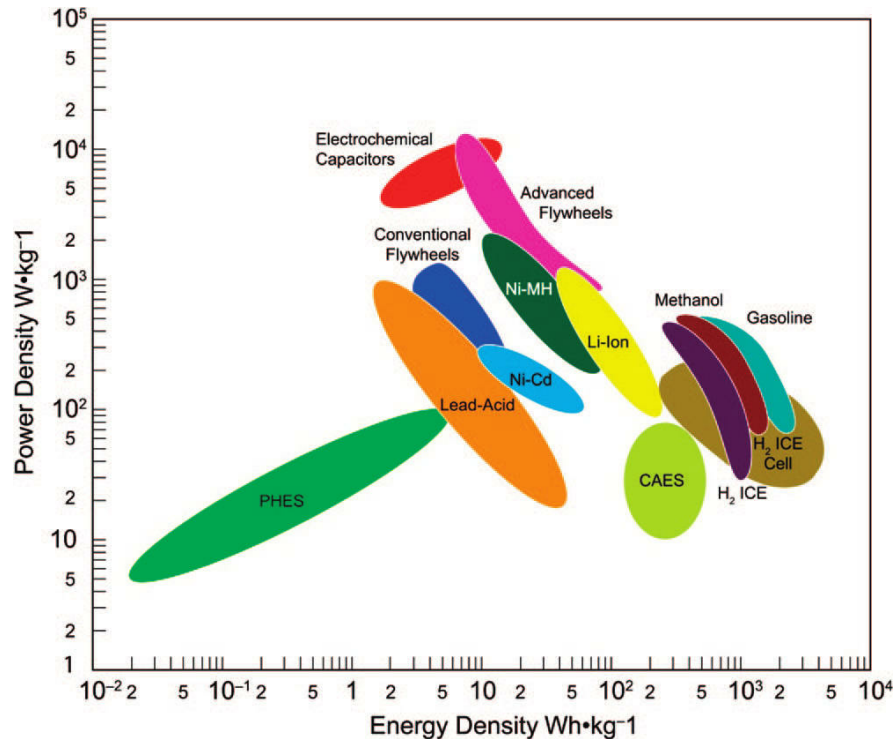


Figure 1.2: Methods of storing solar energy, compared by plotting power density against energy density.

Energy density describes the amount of energy can be stored per unit mass (other densities such as energy per unit volume can also be considered). Power density describes how quickly energy can be moved into or out of the system per unit mass. Ideal fuels for solar energy storage are located at the right in this figure. They have the highest energy density, stored in the form of electrons or chemical bonds.^{8,12} Conventional fuels, such as gasoline, have been attractive as a result of their high energy and power densities; they are also a result of ancient solar energy capture.¹¹

Molecular hydrogen has qualities similar to that of these fuels. Because of this, and the fact that it can be generated from the splitting of water, there has been interest in its production.

1.3 Transition Metal Complexes in Solar Energy Conversion

Transition metals have long been used in catalysis of chemical transformations. The photochemical properties of transition metal complexes have been known for centuries.¹³ During the past century, it was found that in photosynthesis, Photosystem II performs water oxidation at a Mn cluster.¹⁴ Protons produced are then reduced to a hydrogen analogue at Photosystem I.⁸ Catalysts are sought that can, like photosynthesis, perform water splitting. There has been much research in this area.¹⁵ Examples range from the first designed water oxidation catalyst, the “blue dimer”,^{16,17} to homogeneous iron catalysts¹⁸ to multicomponent photovoltaic cells utilizing cobalt-borate catalysts.¹⁹ Some homogeneous ruthenium-based systems have also been reported recently.^{20,21} However, water splitting involves both a complex 4-electron process and proton transfer. HX splitting, where X is a halide, is analogous to water splitting but is only a 2-electron process; thus, it should be a simpler system for investigation.²² Furthermore, the energy storage potential in HX systems is comparable to that in water splitting.¹² In 2001 Nocera and coworkers demonstrated dirhodium complexes that could photocatalytically produce H₂ from HX.²³ A general scheme for this process is shown in Figure 1.1.

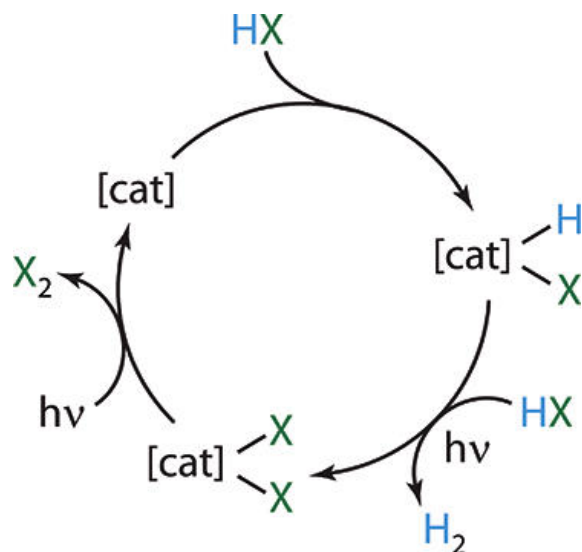


Figure 1.1: Photocatalytic splitting of HX to form H₂ and X₂.

HX is first oxidatively added to the catalyst. Upon further addition of HX in the presence of light, H₂ is produced, leaving a dihalide complex. To close the cycle, the catalyst must be restored to its initial state by removal of the halides through photochemical elimination. This transformation involves M-X bond activation and requires energy; it is a critical step in the catalytic cycle.^{12,24} Nickel complexes have been reported that undergo addition of HX followed by elimination of H₂; however, they were not able to carry out this last step.²⁵

1.4 Gold in Catalysis and Photochemistry

Gold is a late transition metal and a more oxidizing metal center, with a well-studied photochemistry, making it an attractive candidate for the reductive elimination step.^{12,26,27} Towards understanding this transformation, complexes of platinum and gold have been shown to effectively undergo halogen photoreductive elimination.¹² More recently, phosphine-based gold(III) halide complexes have been shown to

photoreductively eliminate X_2 for $X = \text{Cl}$ and Br .²⁴ Here it was shown that solar energy could drive the uphill reduction of gold(III) dihalides to gold(I) complexes, generating an equivalent of Cl_2 in the process through photoreductive elimination. These complexes were shown to give much higher quantum yields than the earlier dirhodium complexes, reinforcing the potential for gold complexes in these applications.²⁴

N-Heterocyclic Carbenes (NHCs) have been studied extensively since the 1960s, and were first shown to ligate metals in 1968.^{28,29} One of the earliest NHC-gold complexes was reported in 1974 by Lappert and coworkers.³⁰ NHC ligands tend to be stronger σ -donors, have greater stability, and are easier to synthesize than their phosphine counterparts; they are also easily modified.³¹ For these reasons, they are attractive ligand systems for potential halogen photoreductive elimination chemistry. The syntheses of many of these types of compounds are also well known.³¹⁻³⁵

Chapter 2

SYNTHESIS AND CHARACTERIZATION OF NHC-GOLD(I)/(III) CHLORIDE COMPLEXES FOR ENERGY STORAGE

2.1 Introduction

Our system (Figure 2.1) was inspired by Nocera's gold-phosphine system. We wanted to investigate whether an analogous system with NHC backbones would display similar results of energetically-uphill photoreductive elimination and energetically-downhill oxidative addition of Cl_2 . (dichloro- λ^3 -iodanyl)benzene (PhICl_2) was chosen as the delivery system for Cl_2 ; it is easily synthesized from iodobenzene and bleach.³⁶

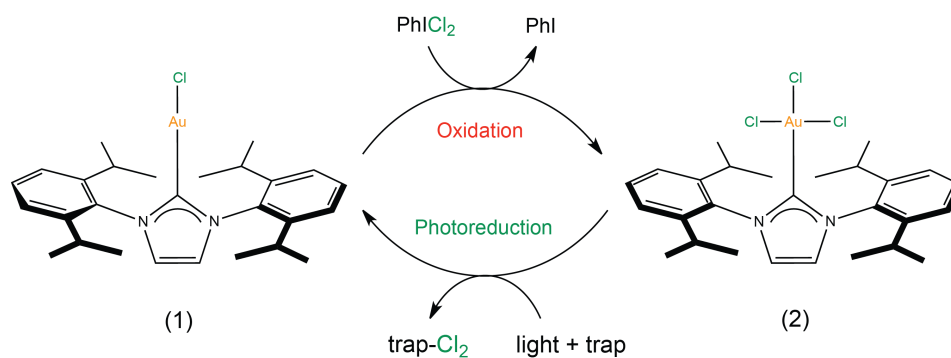


Figure 2.1: Proposed photochemical cycle of NHC-gold(I) and (III) couples. The gold(I) complex (1) is oxidized *via* PhICl_2 to the gold(III) complex (2), which then undergoes photoreductive elimination to reform the starting material.

Furthermore, since NHC-nickel complexes have been shown to undergo oxidative addition of an equivalent of HCl and subsequent photoreductive elimination of H₂ but were unable to perform the crucial halogen photoreductive elimination step,²⁵ we wanted to investigate whether our gold(I)/(III) NHC systems could support this chemistry.

2.2 Results and Discussion

2.2.1 NHC-Gold Chloride Complexes

The synthetic route to the gold(I) chloride complex was very simple, and the oxidation to the gold(III) complex was performed in high yield. 1,3-bis(2,6-diisopropylphenyl)imidazol-2-ylidene (IPr) and 1,3-bis(2,4,5-trimethylphenyl)imidazol-2-ylidene (IMes) were initially investigated as potential NHC ligands. IPr proved to have both a more facile synthetic route and more promising photochemistry, so it was chosen for all further studies.

The photoreduction of the gold(III) complex was then investigated. The complex showed a clean reduction over 30 minutes of exposure to visible light, with the reduction nearly complete after 2 hours (Figure 2.2). The UV-vis spectrum displayed a relatively well-anchored isosbestic point at approximately 272 nm, suggesting that few side products or intermediates were produced. The reaction also proceeded without a trap present, suggesting that either the solvent (CDCl₃) played a role in accepting the eliminated chloride or that Cl₂ was produced and escaped. A time-course ¹H NMR experiment further showed the photochemical reduction (Figure 2.3).

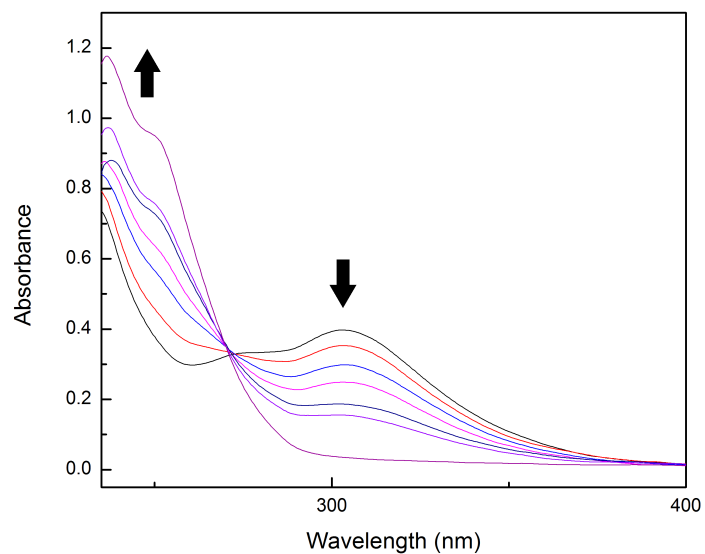


Figure 2.2: UV-Vis time-course spectra for the photochemical reduction of $\text{AuCl}_3(\text{IPr})$ to $\text{AuCl}(\text{IPr})$ in dichloromethane (1.0 cm cuvette) over 2 hours.

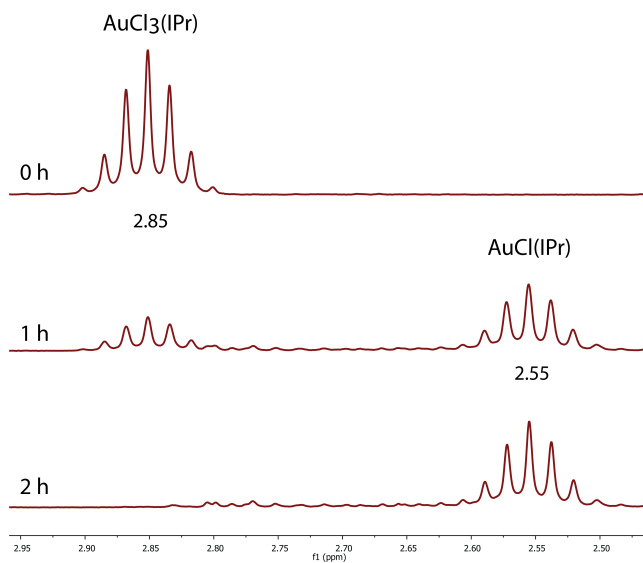


Figure 2.3: ^1H NMR time-course photoreduction of $\text{AuCl}_3(\text{IPr})$ to $\text{AuCl}(\text{IPr})$ over 2 hours. 400 MHz, CDCl_3 .

The results from a ^1H NMR experiment with an internal standard suggested that the yield for the photoreduction in CDCl_3 was approximately 60% after 2 hours of irradiation. This yield is relatively low for potential fuel storage applications.

2.3 Conclusions

The results from these experiments showed that NHC-gold complexes could indeed perform the crucial halogen photoreductive elimination step, and allowed for a proof-of-concept system where solar energy could be stored *via* the endothermic reductive elimination of Cl_2 and released *via* the exothermic addition of Cl_2 . More work is needed on this system to increase the yield of the photoreductive step; this currently would represent a bottleneck in potential applications for energy conversion or catalysis. This system is also supported by a recent report from Monkowius and coworkers of similar NHC-Au bromide complexes that undergo photoreductive elimination. However, both that system and ours require relatively high-energy light; the Au(III) complexes do not absorb at wavelengths greater than ~ 400 nm, leaving a large part of the solar spectrum unutilized. To this end more exploration is needed to harness longer-wavelength light.

2.4 Experimental

2.4.1 General Considerations

Reactions were carried out under air unless otherwise noted. ^1H NMR spectra were recorded at 400 MHz on Bruker spectrometers and were referenced to the residual solvent peak at 7.26 ppm (CDCl_3). ^{13}C NMR spectra were recorded at 100 MHz and referenced to the residual solvent peak at 77.16 ppm (CDCl_3). Gas chromatography - mass spectrometry experiments were performed on an Agilent 6850

series GC system with 5973 Network Mass Selective Detector with EI ion source. Solvents were used directly from commercial sources (VWR) without further purification. UV-vis spectra were recorded on a StellarNet fiber optic UV-Vis spectrophotometer between 190 nm and 1078.5 nm with a 1.0 cm quartz cuvette.

2.4.2 Synthesis of NHC-Gold Chloride Complexes

Synthesis of AuCl(IPr). The corresponding NHC-silver(I) complex was reacted with AuClSC₄H₈ according to the literature.³² Yield: 60%. ¹H NMR (400 MHz, CDCl₃) δ 7.50 (t, *J* = 7.8 Hz, 2H, CH aromatic), 7.29 (d, *J* = 7.8 Hz, 4H, CH aromatic), 7.17 (s, 2H, CH imidazole), 2.55 (sept, *J* = 6.9 Hz, 4H, CH(CH₃)₂), 1.34 (d, *J* = 6.9 Hz, 12H, CH(CH₃)₂), 1.22 (d, *J* = 6.9 Hz, 12H, CH(CH₃)₂).

Synthesis of AuCl₃(IPr). The gold(I) chloride complex (225 mg, 0.362 mmol) was added to 4 mL of dichloromethane in a 50 mL round bottom flask. PhICl₂ (110 mg, 0.399 mmol) was added, the flask was covered with foil, and the solution was stirred for 1 day. The volume was reduced by half, ~ 10 mL hexanes were added, and the product was isolated by filtration as an off-white powder. Yield: 0.241 g (96%). ¹H NMR (400 MHz, CDCl₃) δ 7.56 (t, *J* = 7.8 Hz, 2H, CH aromatic), 7.36 (s, 2H, CH imidazole), 7.35 (s, 4H, CH aromatic), 2.84 (sept, *J* = 6.7 Hz, 4H, CH(CH₃)₂), 1.39 (d, *J* = 6.6 Hz, 12H, CH(CH₃)₂), 1.13 (d, *J* = 6.9 Hz, 12H, CH(CH₃)₂).

2.4.3 Synthesis of NHC-Gold(III) HCl Complexes

The oxidation of the gold(I) chloride complex was attempted with an equivalent of HCl rather than Cl₂ in the form of lutidine·HCl. It was expected that HCl would be oxidatively added to the gold center as with PhICl₂. This was attempted in

chloroform-*d*, acetonitrile-*d*₆, and methanol-*d*₄ from room temperature to 50 °C. In all cases there was no change from the starting material.

2.4.4 Photochemical Studies

Procedures for UV-vis spectroscopy. Spectra were recorded on a StellarNet fiber optic UV-Vis spectrophotometer between 190 nm and 1078.5 nm with a 1.0 cm quartz cuvette. For the photoreduction, a cuvette was filled with approximately 3 mL of a 100 μM solution of AuCl₃(IPr). The solution was exposed to a visible light lamp, and a spectrum was recorded every 5 minutes.

Procedures for NMR photoreduction studies. AuCl₃(IPr) (approx. 10 mg) was dissolved in CDCl₃ and transferred to an NMR tube with a sealed 1,4-dioxane internal standard. Spectra were taken before and 2 hours after irradiation with a visible light lamp.

Chapter 3

SYNTHESIS AND CHARACTERIZATION OF NHC-GOLD(I)/(III) ARYL COMPLEXES

3.1 Introduction

Once the preliminary groundwork had been done on the Au(I) and Au(III) chloride complexes, we set about to investigate the effects of replacing the terminal chloride ligand. If reductive elimination involves the trans chlorides in Au(III) complexes, the terminal ligand should be able to be replaced, and the chemistry of the photoreduction can be tweaked by adjusting the steric and electronic properties of the new ligand. The main limitation in the AuCl₃(IPr) scheme was the small wavelength range of 200-400 nm, which does not take advantage of the full solar spectrum available. Phenyl and fluorinated phenyl derivatives were chosen for these studies in the hopes that this range could be expanded (Figure 3.1).³⁷

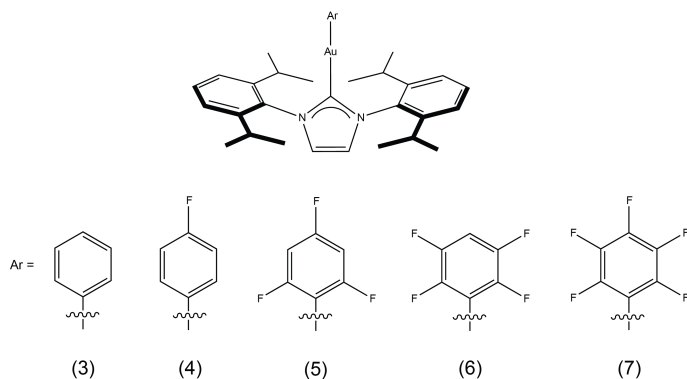


Figure 3.1: Arylgold(I) complexes studied: AuPh(IPr) (3), AuC₆H₄F(IPr) (4), AuC₆H₂F₃(IPr) (5), AuC₆H₂F₄(IPr) (6), and AuC₆F₅(IPr) (7).

It was expected that halogen photoreductive elimination could be observed with these systems as well; Monkowius and coworkers showed that photoreductive elimination chemistry with Au(III) tribromide complexes was also accessible with complexes in which the terminal bromide ligand was replaced with an NHC (Figure 3.2).³⁸

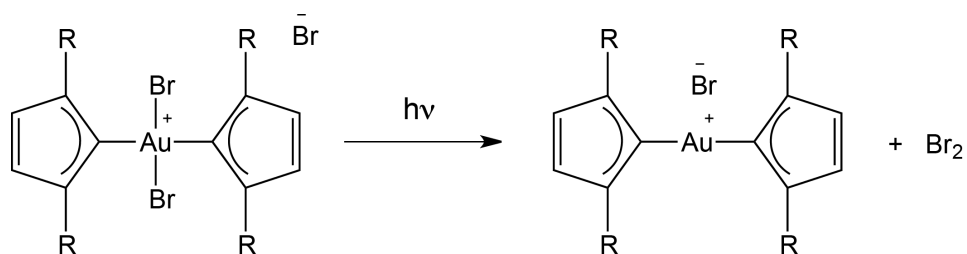


Figure 3.2: Photoreductive halogen elimination from bis-NHC-Au bromide complexes (R = Bn).

3.2 Results and Discussion

3.2.1 Phenyl Derivatives

It was expected that AuPh(IPr) could be oxidized as in the case of AuCl(IPr) to form a gold(III) complex with *trans* chloride ligands. When the oxidation was attempted with PhICl₂, the only material present after roughly ten minutes at room temperature was the starting AuCl(IPr). This was tentatively attributed to reductive elimination of a chlorinated phenyl group and reformation of AuCl(IPr) (Figure 3.3). The ¹³C NMR spectrum of the mixture after reaction was compared with that of authentic chlorobenzene, suggesting that it was indeed present as a result of the reaction (Figure 3.4). When GC-MS was carried out in dichloromethane, chlorobenzene tended to elute with the solvent and was not clearly observed. The

reaction was run again in mesitylene, and GC-MS was performed. Chlorobenzene eluted before the heavier mesitylene, giving a clear peak as confirmation of the reductive elimination product.

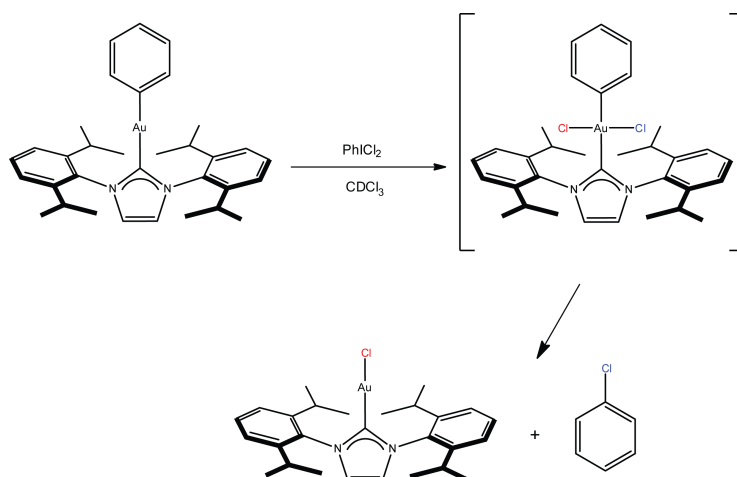


Figure 3.3: Tentative scheme for thermal reductive elimination of AuPh(IPr). The Au(I) complex is oxidized to form the Au(III) complex, which is unstable and quickly undergoes reductive elimination to form AuCl(IPr) and chlorobenzene.

We were not able to observe a gold(III) complex of the form AuPhCl₂(IPr) due to the speed of the reduction; however, it was assumed that this species was formed and quickly reduced. Interestingly, Limbach and coworkers were able to isolate the similar complex AuPhCl₂(IMes), which was stable enough to permit X-ray diffraction studies.³² In that case the oxidation was performed at 0 °C rather than at room temperature. Room temperature may have provided enough thermal energy for the fast reductive elimination observed in the case of AuPh(IPr).

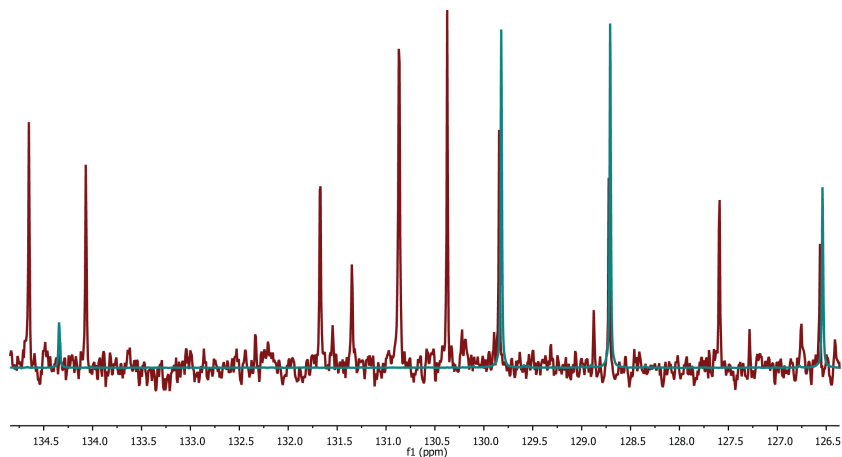


Figure 3.4: ^{13}C NMR of AuPh(IPr) reductive elimination. Two spectra are overlaid; one of the reaction mixture (red) and one of authentic chlorobenzene (blue).

It has been shown that gold(III) alkyl complexes can undergo reductive elimination to form a halogenated product.³⁹ Further, aryl halogenations have been demonstrated with gold(III) catalysts and *N*-Halosuccinimides.⁴⁰ Because photoreductive elimination was observed to produce chlorinated aryl molecules in our system, we wanted to investigate whether the two-step process from the arylboronic acid to the chlorinated aryl could be performed catalytically. In the catalytic studies, none of the chlorinated aryl product was observed by ^{13}C NMR. It was found that there was a small amount of the gold(I) phenyl complex formed and a larger amount of the gold(III) trichloride complex. Most likely, since the oxidation of AuCl(IPr) is a much faster process than the formation of AuPh(IPr), this step proceeded first, preventing the system from working catalytically. Possible ways to circumvent this undesired reactivity could involve staggered additions of oxidant, different solvent systems, or a different oxidant altogether.

3.2.2 Fluorinated Phenyl Derivatives

The electronic effects of the terminal aryl ligand were investigated by varying the number of electron-withdrawing fluorines: 1 (4-fluorophenyl), 3 (2,4,6-trifluorophenyl), 4 (2,3,5,6-tetrafluorophenyl) and 5 (pentafluorophenyl). Because of the varying acidity of the proton to be removed from the fluorinated benzene starting material, two procedures were used for the synthesis of the Au(I) aryl derivatives. Tri-, tetra- and pentafluoro derivatives involved removing protons acidic enough to facilitate a straightforward acid-base reaction.⁴¹ For the monofluorophenyl derivative a boronic acid of the desired group was required due to the lower acidity of the aryl proton.³⁷

The pentafluorophenyl derivative $\text{AuC}_6\text{F}_5(\text{IPr})$, most electronically different than the phenyl derivative, was first investigated. The methodology of oxidation via PhICl_2 was successful for $\text{AuC}_6\text{F}_5(\text{IPr})$, the complex with the most electron-deficient aryl ligand. The reaction was nearly complete after 12 hours, and the complex was stable enough that crystals could be grown for X-ray diffraction, showing the chloride ligands *trans* to one another (Figure 3.5). The structure of $\text{AuC}_6\text{F}_5(\text{IPr})$ is also shown. Crystal data and structure refinement are summarized in the appendix.

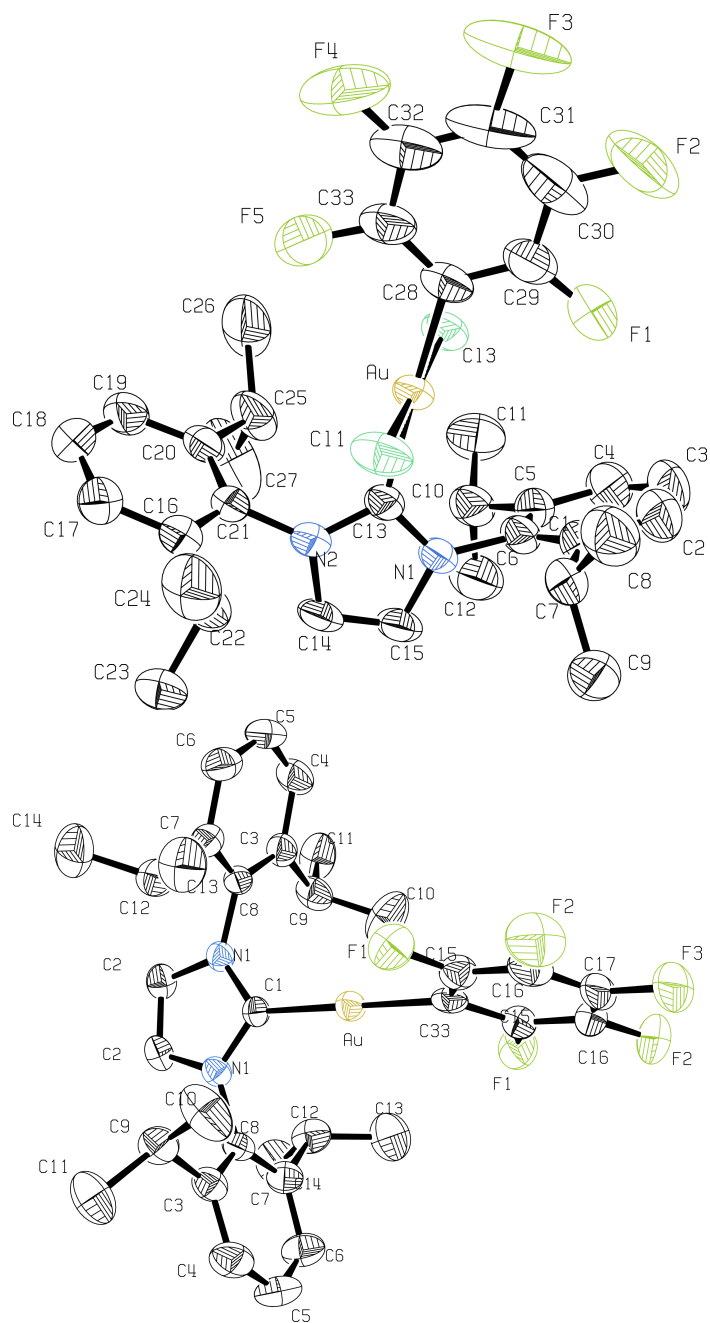


Figure 3.5: The molecular structures of $\text{AuC}_6\text{F}_5\text{Cl}_2(\text{IPr})$ (top) and $\text{AuC}_6\text{F}_5(\text{IPr})$ (bottom), with ellipsoids depicted at the 30% probability level. H atoms have been omitted for clarity.

Once the electronic endpoints of the study had been explored, we set about to investigate the complexes with intermediately electron-deficient ligands. The oxidation was first attempted with the monofluorophenyl derivative $\text{AuC}_6\text{H}_4\text{F}(\text{IPr})$. Similar to $\text{AuPh}(\text{IPr})$, no oxidized aryl product was observed by ^1H NMR after 10 minutes at room temperature; only $\text{AuCl}(\text{IPr})$ was present (Figure 3.6). The reductive elimination product 1-chloro-4-fluorobenzene was observed by GC-MS. The oxidation was repeated at $0\text{ }^\circ\text{C}$ to see if the $\text{Au}(\text{III})$ aryl complex could be formed at a lower temperature, but again only $\text{AuCl}(\text{IPr})$ and $\text{AuCl}_3(\text{IPr})$ were observed (the latter forming from $\text{AuCl}(\text{IPr})$ and excess oxidant in solution). However, it is possible that the $\text{Au}(\text{III})$ aryl complex could indeed have formed, but that the sample could have warmed enough in the roughly 10-minute movement to the NMR spectrometer for reductive elimination to occur. This experiment will need to be repeated more carefully to confirm this result.

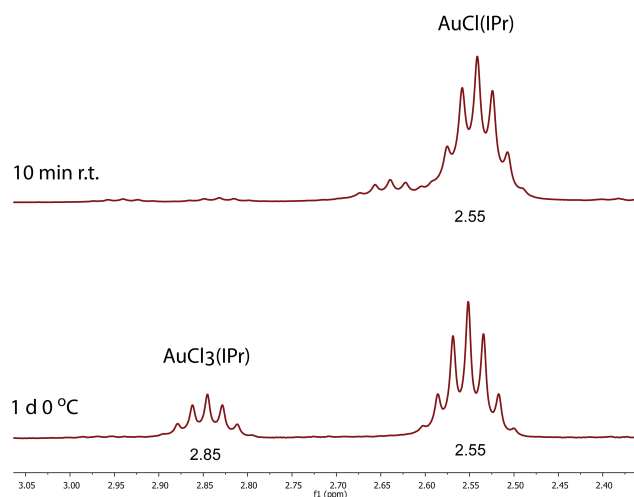


Figure 3.6: ^1H NMR spectra of $\text{AuC}_6\text{F}(\text{IPr})$ after oxidation with PhICl_2 under two different conditions. The spectra have been truncated to show the characteristic isopropyl H septet. CDCl_3 , 400 MHz.

The oxidation was then attempted with the trifluorophenyl derivative. Because its electronic character is between that of the phenyl and pentafluorophenyl derivatives, it was expected that this complex would form some of the gold(III) species but also undergo some thermal reductive elimination; this was indeed seen by NMR (Figure 3.7). After 4 hours at 55 °C with PhICl₂, there was an oxidized arylgold(III) species present, but in a roughly 2:1 ratio with AuCl(IPr). Some AuCl₃(IPr) was also present (excess PhICl₂ oxidized AuCl(IPr) once it had been formed). This showed that AuC₆H₂F₃Cl₂(IPr) was stable enough to exist on a long enough timescale to be observed, but that it still could follow a thermal elimination pathway to some extent. The oxidation was then performed for 2 days at room temperature, resulting in the same species present, but with the Au(III) aryl in an approximately 6:1 ratio with AuCl(IPr). This highlights the thermal nature of the elimination pathway; at a lower temperature a smaller extent of reductive elimination is observed.

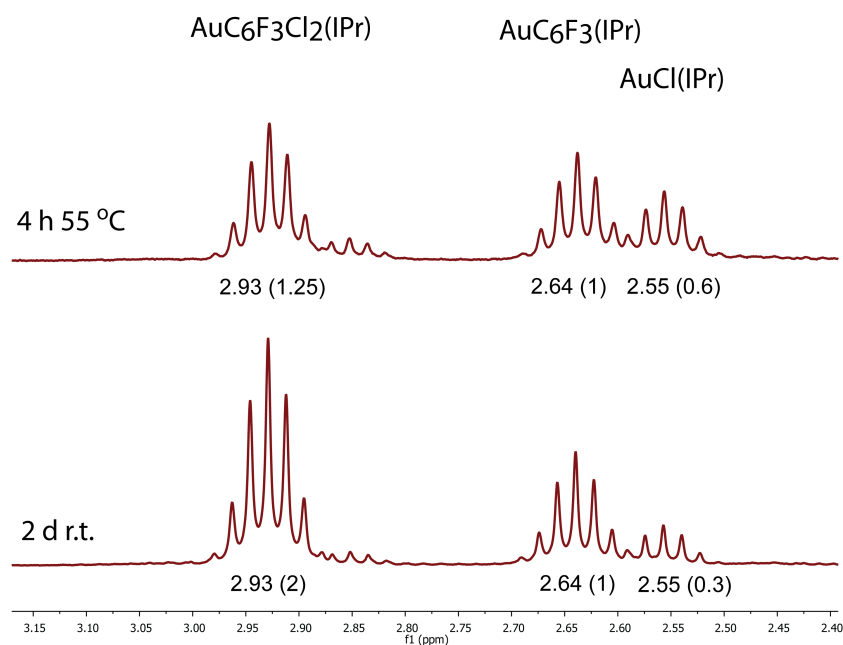


Figure 3.7: ¹H NMR spectra of AuC₆H₂F₃(IPr) after oxidation under two different conditions. The spectra have been truncated to show the characteristic isopropyl H septet. CDCl₃, 400 MHz.

Oxidation of AuC₆HF₄(IPr) at room temperature for 2 days yielded only the oxidized aryl product. Further heating at 35 °C for 5 hours resulted in a larger extent of oxidation, but only when the oxidation was performed at 55 °C for 4 hours was a trace of AuCl(IPr) seen (Figure 3.8).

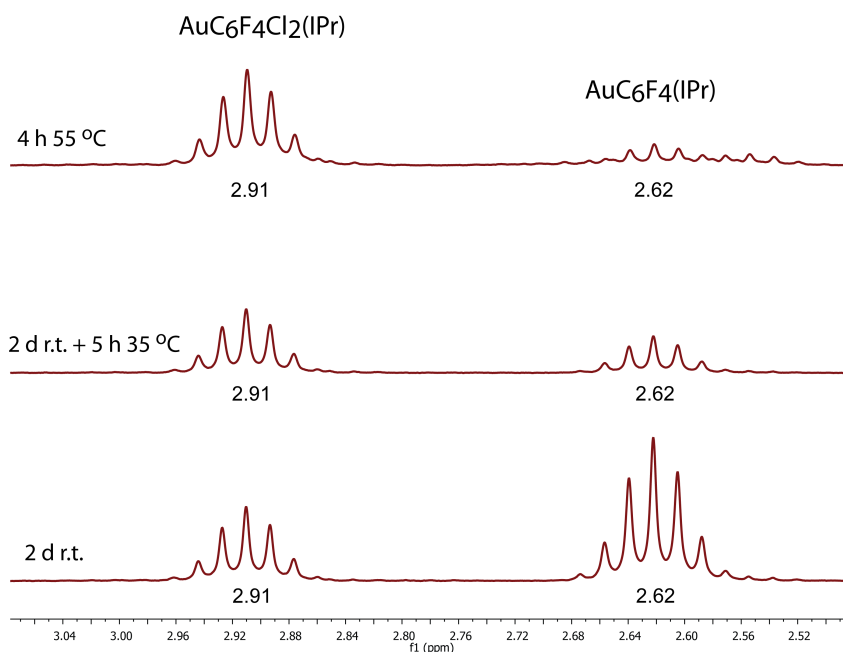


Figure 3.8: ^1H NMR spectra of $\text{AuC}_6\text{HF}_4(\text{IPr})$ after oxidation under various conditions. The spectra have been truncated to show the characteristic isopropyl H septet. CDCl_3 , 400 MHz.

After oxidation $\text{AuC}_6\text{F}_5(\text{IPr})$ yielded only the gold(III) complex. The oxidation reaction was not complete after 8 hours at 50 °C, but could complete after 3 days at room temperature. In both cases, no thermal reduction to $\text{AuCl}(\text{IPr})$ was observed.

To investigate the photochemical properties of this oxidized complex ($\text{AuC}_6\text{F}_5\text{Cl}_2(\text{IPr})$), a 20-hour time-course UV-vis experiment was set up (Figure 3.9). This showed a well-anchored isosbestic point at approximately 265 nm, suggesting a clean reduction to the gold(I) complex with few side products and no intermediates. A ^1H NMR time-course experiment also showed a clean reduction (Figure 3.10). However, according to ^1H NMR, the resulting gold(I) complex was again the original $\text{AuCl}(\text{IPr})$, and not the anticipated $\text{AuC}_6\text{F}_5(\text{IPr})$. GC-MS confirmed that the complex

was again undergoing reductive elimination to produce the chlorinated aryl and the gold(I) chloride complex. As opposed to the phenyl derivative AuPh(IPr), this fully fluorinated complex showed excellent thermal stability after oxidation to gold(III). However, no expansion in the wavelength range was seen; the effective range for this complex was even smaller than that of AuCl₃(IPr) at 200-350 nm.

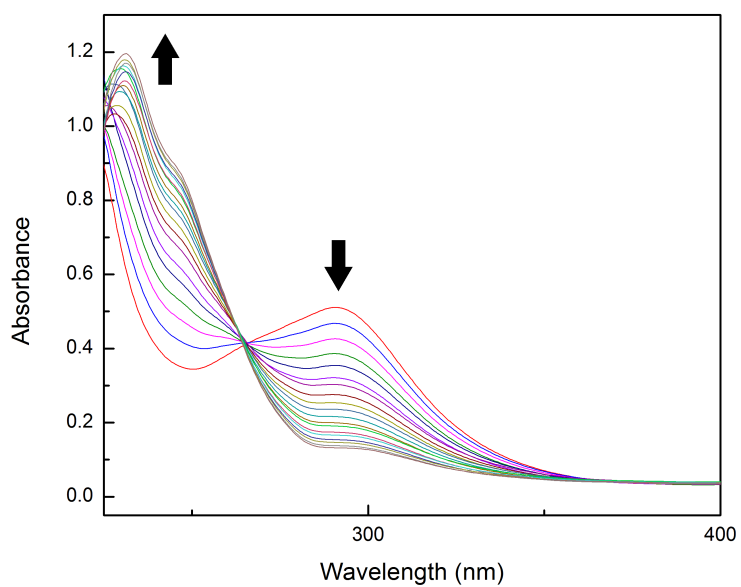


Figure 3.9: UV-Vis time-course photoreduction over 20 hours for AuC₆F₅Cl₂(IPr). Spectra were taken every hour.

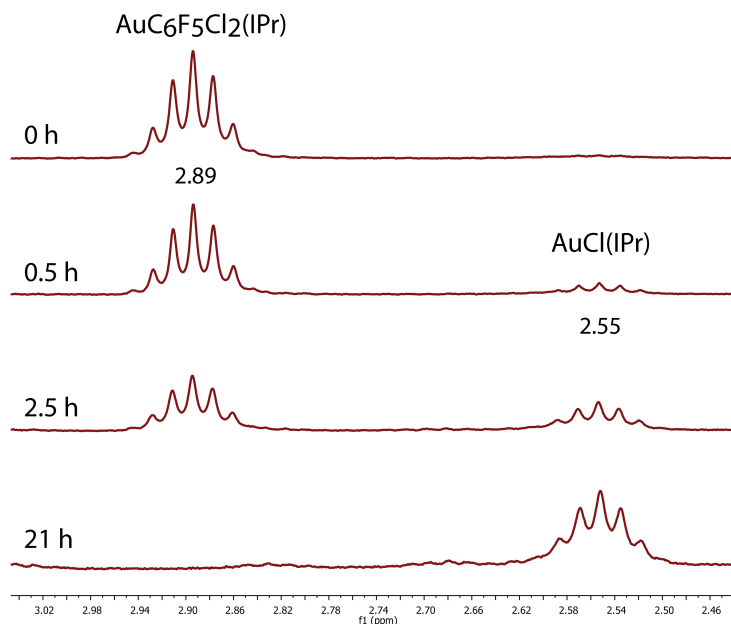


Figure 3.10: ^1H NMR time-course photoreduction for $\text{AuC}_6\text{F}_5\text{Cl}_2(\text{IPr})$ over 21 hrs, truncated to show the characteristic isopropyl H septet. All integrals were normalized to a 1,4-dioxane internal standard ($\delta = 3.7$). CDCl_3 , 400 MHz.

The photoreduction was repeated with the oxidized tri- and tetrafluorophenyl derivatives. Time-course NMR spectra for the photoreduction of $\text{AuC}_6\text{H}_2\text{F}_3\text{Cl}_2(\text{IPr})$ and $\text{AuC}_6\text{HF}_4\text{Cl}_2(\text{IPr})$ showed results similar to the pentafluorophenyl derivative upon irradiation and are provided in the appendix. Once again, GC-MS experiments confirmed that reductive elimination produced the chlorinated fluorophenyl product in each case (1-chloro-2,4,6-trifluorobenzene and 1-chloro-2,3,5,6-tetrafluorobenzene, respectively).

3.3 Conclusions

These systems are very interesting in that there are two pathways for reductive elimination: thermal and photochemical. The electronics of the terminal aryl ligand seems to determine which pathway is preferred. The gold(III) complex with the least electron-withdrawing ligand (phenyl) proceeded very quickly by thermal reductive elimination. The one with the most electron-withdrawing (pentafluorophenyl) showed enough stability to form crystals and keep for long times and displayed a photochemical transformation, producing the reductive elimination product only upon irradiation. It was expected that the trifluorophenyl derivative, in between the phenyl and pentafluorophenyl electronically, would follow both pathways to some extent, and this was indeed demonstrated. The reductive elimination pathways of the monofluorophenyl and tetrafluorophenyl derivatives fit nicely into the proposed ligand electronics gradient.

Analogous to previous mechanistic studies on reductive elimination from Au(III) complexes, these Au(III) aryl systems most likely undergo elimination from a 3-coordinate T-shaped complex.^{39,42,43} From the d^8 square planar Au(III) complexes, this involves the first step of dissociation of a Cl to form the 3-coordinate intermediate. Qualitatively, the more electron density is placed on the Au center, the more labile the Cl should be. Thus, for the more electron-donating Phenyl and monofluorophenyl complexes, this could explain the fast reductive eliminations. The opposite is true for the lack of thermal reactivity for the complexes with electron-withdrawing aryl ligands. However, their reactivity with light can be rationalized by comparison with the light-driven removal of Cl from $Au^{III}Cl_3$.²⁶ A similar mechanism could drive the formation of the 3-coordinate intermediate, which then would undergo reductive elimination.

There is also the possibility of a steric effect to explain the difference in reactivities. However, this was ruled out, as the trifluoro- and pentafluorophenyl derivatives showed very different oxidation chemistry, yet had similar steric bulk around the gold center. The only difference in the trifluorophenyl derivative is the lack of two fluorines in the *meta* position relative to the gold center; this should not affect the reactivity from a steric perspective.

While these systems did not show the type of desired photochemistry seen in the original AuCl₃(IPr) – AuCl(IPr) system, this represents an important step in understanding the effects of electronics in the ligand from an energy perspective. X-X bond formation is wanted rather than C-X for solar energy storage, and this system gives some insight into the mechanism by which C-X bond formation takes place.

The ability to selectively chlorinate aryl groups is attractive from a catalytic standpoint; there has been much work in this area.⁴⁴ However, we were unable to observe catalytic activity under the conditions explored in these limited experiments. In 2010 Wang and coworkers studied AuCl₃ as a catalyst for such reactions, but many of the reactions required high catalyst loading, long times or high temperatures.⁴⁰ Further study of our system in catalysis could potentially improve these results. Potential avenues of exploration involve varying solvent conditions, oxidants, and experimental setup, such as the possibility of staggered additions of reactants.

3.4 Future Work

One of the most promising avenues for these systems is in fluorination chemistry. It has been demonstrated here that selective chlorination is possible for aryl systems. Fluorinations are more difficult synthetically, and efficient catalysis of this type could prove important commercially; Toste and coworkers recently reported

alkylgold(III) fluoride complexes, achieved through oxidation with XeF₂.^{45,46} The Alkylgold(III) and Cycloalkylgold(III) complexes reported underwent reductive elimination to form C-F bonds in much the same manner as our system (Figure 3.11). If this methodology could be applied to arylgold complexes as well, it could represent a step toward new catalysts for C-F bond formation.

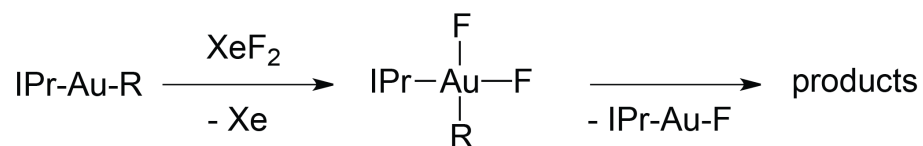


Figure 3.11: Reductive elimination in alkylgold(III) fluoride complexes.

Finally, the complexes with electron-withdrawing ligands reported here showed increased photochemical activity, but the photoreductive elimination occurred on relatively slow timescales (upwards of 8-12 hours). The addition of light-harvesting groups to the NHC backbone could lead to more efficient photoreduction. Large light-active molecules such as BODIPY or porphyrins could potentially improve LMCT, facilitating faster reductive elimination.

3.5 Experimental

3.5.1 General Considerations

Reactions were carried out under air unless otherwise noted. ¹H NMR spectra were recorded at 400 MHz on Bruker spectrometers and were referenced to the residual solvent peak at 7.26 ppm (CDCl₃), 3.31 ppm (CD₃OD), 7.16 ppm (C₆D₆) or

1.94 ppm (CD₃CN). ¹³C NMR spectra were recorded at 100 MHz and referenced to the residual solvent peak at 77.16 ppm (CDCl₃), 49.00 ppm (CD₃OD), 128.06 ppm (C₆D₆) or 118.26 ppm (CD₃CN). Gas chromatography - mass spectrometry experiments were performed on an Agilent 6850 series GC system with 5973 Network Mass Selective Detector with EI ion source. Solvents were used directly from commercial sources (VWR) without further purification. UV-vis spectra were recorded on a StellarNet fiber optic UV-Vis spectrophotometer between 190 nm and 1078.5 nm with a 1.0 cm quartz cuvette. Stock solutions were prepared at 150 μM and diluted to appropriate concentrations.

3.5.2 Synthesis of NHC-Arylgold Complexes

Synthesis of AuPh(IPr). To a solution of AuCl(IPr) (100 mg, 0.161 mmol) in isopropanol (5 mL) were added phenylboronic acid (42.6 mg, 0.349 mmol) and cesium carbonate (110 mg, 0.338 mmol). After stirring at 55 °C for 24 hrs under an atmosphere of nitrogen, the reaction mixture was cooled and the solvent was removed under vacuum. The resulting mixture was extracted into benzene and filtered through celite. The resulting solution was evaporated to a residue, azeotroped with pentane, and evaporated to dryness. This was repeated, and the resulting solid was dissolved into minimal benzene. This solution was dropped into pentane and held at -40 °C for 2 days. The resulting solid was collected and dried under vacuum to afford AuPh(IPr) as a white powder. The filtrate was held at -40 °C for a further day to yield more product. Yield: 71 mg (66%). ¹H NMR (400 MHz) (CDCl₃): δ 7.46 (t, *J* = 7.8 Hz, 2H, *CH* aromatic), 7.27 (d, *J* = 8.8 Hz, 4H, *CH* aromatic), 7.14 (s, 2H, *CH* imidazole), 7.07 (dd, *J* = 6.3 Hz, 1.5 Hz, 2H, *CH* phenyl), 7.00 (t, *J* = 7.44 Hz, 2H, *CH* phenyl), 6.83 (tt, *J* = 7.3 Hz, 1.5 Hz, 1H, *CH* phenyl), 2.66 (sept, *J* = 6.9 Hz, 4H, *CH*(CH₃)₂), 1.40

(d, $J = 6.8$ Hz, 12H, CH(CH₃)₂), 1.24 (d, $J = 6.9$ Hz, 12H, CH(CH₃)₂) ppm. ¹³C NMR (101 MHz, CDCl₃) δ 196.99, 169.85, 145.85, 140.62, 134.71, 130.24, 126.77, 124.32, 124.04, 122.84, 77.16, 28.90, 24.67, 24.04.

Synthesis of AuC₆F₅(IPr). To a vial were added AuCl(IPr) (74.6 mg, 0.12 mmol), pivalic acid (30.6 mg, 0.30 mmol), potassium carbonate (29.4 mg, 0.21 mmol), silver(I) oxide (21 mg, 0.09 mmol), pentafluorobenzene (60 μ L, 0.54 mmol) and dimethylformamide (0.6 mL). After stirring at 55 °C for 4.5 hrs, the reaction mixture was cooled and filtered. The solvent was removed under vacuum, and the residue was azeotroped with hexanes. After removing the solvent, the pipette filter was washed with dichloromethane onto the residue, and the solvent was again removed. The mixture was purified by column chromatography on silica with eluent of 3:1 hexanes:dichloromethane to afford AuC₆F₅(IPr) as a white solid. Yield: 58 mg (64%) ¹H NMR (400 MHz, CDCl₃): δ 7.49 (t, $J = 7.8$ Hz, 2H, CH aromatic), 7.29 (d, $J = 7.8$ Hz, 4H, CH aromatic), 7.20 (s, 2H, CH imidazole), 2.61 (sept, $J = 6.9$ Hz, 4H, CH(CH₃)₂), 1.36 (d, $J = 6.9$ Hz, 12H, CH(CH₃)₂), 1.24 (d, $J = 6.9$ Hz, 12H, CH(CH₃)₂). ¹³C NMR (101 MHz, CDCl₃) δ 191.97, 150.23, 147.97, 145.89, 139.35, 137.97, 136.98, 135.52, 134.20, 130.59, 124.14, 123.13, 77.16, 28.98, 24.50, 24.13.

Synthesis of AuC₆F₅Cl₂(IPr). To a solution of AuC₆F₅(IPr) (138 mg, 0.18 mmol) in chloroform (20 mL) was added (dichloro- λ 3-iodanyl)benzene (176.5 mg, 0.64 mmol). The reaction mixture was heated to 45 °C for 3 hrs. After cooling, the solvent was removed under vacuum. The product was isolated by column chromatography on silica with eluent of 2:1 hexanes:dichloromethane to afford AuC₆F₅Cl₂(IPr) as a white solid. Yield: 114.2 mg (75%). ¹H NMR (400 MHz, CDCl₃) δ 7.57 (t, $J = 7.8$ Hz, 2H, CH aromatic), 7.39 (d, $J = 7.8$ Hz, 4H, CH aromatic), 7.32

(s, 2H, CH imidazole), 2.90 (sept, $J = 6.7$ Hz, 4H, $\text{CH}(\text{CH}_3)_2$), 1.41 (d, $J = 6.7$ Hz, 12H, $\text{CH}(\text{CH}_3)_2$), 1.15 (d, $J = 6.9$ Hz, 12H, $\text{CH}(\text{CH}_3)_2$). ^{13}C NMR (101 MHz, CDCl_3) δ 168.35, 146.08, 144.04, 140.64, 138.46, 136.00, 132.89, 131.41, 125.37, 124.45, 113.19, 77.16, 29.14, 26.73, 22.59.

Synthesis of $\text{AuC}_6\text{H}_4\text{F}(\text{IPr})$. To a solution of $\text{AuCl}(\text{IPr})$ (121.5 mg, 0.20 mmol) in isopropanol (5 mL) in a round bottom flask were added 4-fluorophenylboronic acid (58.8 mg, 0.42 mmol) and cesium carbonate (132 mg, 0.41 mmol). The flask was evacuated and charged with nitrogen and stirred at 55 °C for 24 hrs. The reaction mixture was cooled and the solvent was removed under vacuum. The resulting mixture was extracted into benzene and filtered through celite. The resulting solution was evaporated to a residue, azeotroped with dichloromethane, and evaporated to dryness. Minimal dichloromethane was added and the solvent volume was reduced until precipitate formed. Hexanes were added and the solid was collected by filtration and dried under vacuum to afford $\text{AuC}_6\text{H}_4\text{F}(\text{IPr})$ as a white powder. Yield: 43.7 mg (33%). ^1H NMR (400 MHz, CDCl_3) δ 7.46 (t, $J = 7.8$ Hz, 2H, CH aromatic), 7.28 (s, 2H, CH aromatic), 7.14 (s, 2H, CH imidazole), 7.00 (t, $J = 7.9$ Hz, 2H, CH aryl), 6.72 (dd, $J = 10.3, 8.4$ Hz, 2H, CH aryl), 2.65 (sept, $J = 6.9$ Hz, 4H, $\text{CH}(\text{CH}_3)_2$), 1.39 (d, $J = 6.9$ Hz, 12H, $\text{CH}(\text{CH}_3)_2$), 1.23 (d, $J = 6.9$ Hz, 12H, $\text{CH}(\text{CH}_3)_2$).

Synthesis of $\text{AuC}_6\text{H}_2\text{F}_3(\text{IPr})$. To a vial were added $\text{AuCl}(\text{IPr})$ (74.6 mg, 0.12 mmol), pivalic acid (30.6 mg, 0.30 mmol), potassium carbonate (29.4 mg, 0.21 mmol), silver(I) oxide (21 mg, 0.09 mmol), 2,4,6-trifluorobenzene (54 μL , 0.54 mmol) and dimethylformamide (0.6 mL). After stirring at 55 °C for 5 hrs, the reaction mixture was cooled and filtered. The solvent was removed under vacuum, and the resulting

residue was azeotroped with dichloromethane. Silica and dichloromethane were then added and the solvent was removed. The mixture was purified by column chromatography on silica with eluent of 90:10 hexanes:dichloromethane to afford $\text{AuC}_6\text{H}_2\text{F}_3(\text{IPr})$ as a white solid. Yield: 43.6 mg (51%). ^1H NMR (400 MHz, CDCl_3) δ 7.48 (t, $J = 7.8$ Hz, 2H, *CH* aromatic), 7.28 (d, $J = 7.8$ Hz, 4H, *CH* aromatic), 7.18 (s, 2H, *CH* imidazole), 6.31 (dd, $J = 9.6, 4.8$ Hz, 2H, *CH* aryl), 2.64 (sept, $J = 6.9$ Hz, 4H, *CH*(CH_3)₂), 1.37 (d, $J = 6.9$ Hz, 12H, *CH*(CH_3)₂), 1.24 (d, $J = 6.9$ Hz, 12H, *CH*(CH_3)₂).

Synthesis of $\text{AuC}_6\text{HF}_4(\text{IPr})$. To a vial were added $\text{AuCl}(\text{IPr})$ (74.6 mg, 0.12 mmol), pivalic acid (30.6 mg, 0.30 mmol), potassium carbonate (29.4 mg, 0.21 mmol), silver(I) oxide (21 mg, 0.09 mmol), 2,3,5,6-tetrafluorobenzene (60 μL , 0.54 mmol) and dimethylformamide (0.6 mL). After stirring at 53 °C for 5 hrs, the reaction mixture was cooled and filtered. The solvent was removed under vacuum, silica and dichloromethane were added, and the solvent was removed. The was purified by column chromatography on silica with eluent of 90:10 hexanes:dichloromethane to afford $\text{AuC}_6\text{HF}_4(\text{IPr})$ as a white solid. Yield: 58 mg (66%). ^1H NMR (400 MHz, CDCl_3) δ 7.49 (t, $J = 7.8$ Hz, 2H, *CH* aromatic), 7.29 (d, $J = 7.8$ Hz, 4H, *CH* aromatic), 7.20 (s, 2H, *CH* imidazole), 6.52 – 6.43 (m, 1H, *CH* aryl), 2.62 (sept, $J = 6.9$ Hz, 4H, *CH*(CH_3)₂), 1.37 (d, $J = 6.9$ Hz, 12H, *CH*(CH_3)₂), 1.24 (d, $J = 6.9$ Hz, 12H, *CH*(CH_3)₂).

Synthesis of $\text{AuC}_6\text{HF}_4\text{Cl}_2(\text{IPr})$. To a vial were added $\text{AuC}_6\text{HF}_4(\text{IPr})$ (35 mg, 0.048 mmol), PhICl_2 (14.3 mg, 0.052 mmol) and dichloromethane (1 mL). The solution was heated to 55 °C for 5.5 hrs. The solution was cooled and solvent was removed under vacuum. By NMR there was a ratio of about 60:40 Au(III):Au(I), so

1.5 mg PhICl_2 were added with 1 mL dichloromethane and the solution was heated to 55 °C for 4 further hrs. The solution was again cooled and solvent removed to yield clean $\text{AuC}_6\text{HF}_4\text{Cl}_2(\text{IPr})$ as an off-white powder. Yield: 35 mg (91%). ^1H NMR (400 MHz, CDCl_3) δ 7.56 (t, $J = 7.8$ Hz, 2H, CH aromatic), 7.38 (d, $J = 7.8$ Hz, 4H, CH aromatic), 7.31 (s, 2H, CH imidazole), 6.68 – 6.58 (m, 1H, CH aryl), 2.91 (sept, $J = 6.8$ Hz, 4H, $\text{CH}(\text{CH}_3)_2$), 1.41 (d, $J = 6.6$ Hz, 12H, $\text{CH}(\text{CH}_3)_2$), 1.15 (d, $J = 6.8$ Hz, 12H, $\text{CH}(\text{CH}_3)_2$).

3.5.3 Photochemical Studies

Procedures for UV-vis spectroscopy. Spectra were recorded on a StellarNet fiber optic UV-Vis spectrophotometer between 190 nm and 1078.5 nm with a 1.0 cm quartz cuvette. For the time-course photoreduction, a cuvette was filled with approximately 3 mL of a 100 μM solution of $\text{AuCl}_2\text{C}_6\text{F}_5(\text{IPr})$ (diluted from a 150 μM stock solution). The top of the cuvette was exposed to a visible-light lamp perpendicular to the detector, and the solution was stirred to ensure constant mixing.

Procedures for NMR photoreduction studies. Gold(III) complexes were dissolved in CDCl_3 and transferred to an NMR tube with a sealed 1,4-dioxane internal standard. The sample was placed in front of a visible-light lamp, and spectra were recorded at given time intervals.

3.5.4 Catalytic Studies

All reactions were performed in NMR tubes with deuterated solvents. A control was performed with phenylboronic acid (5.3 mg, 0.044 mmol) and PhICl_2 (12 mg, 0.044 mmol) in CDCl_3 . No reaction was observed by ^{13}C NMR at room temperature, and further heating overnight at 50 °C did not promote a reaction. Next,

the experiment was repeated in CDCl_3 and CD_3OD with $\text{AuCl}(\text{IPr})$ (3 mg, 4.8 mmol), $\text{PhB}(\text{OH})_2$ (5.9 mg, 48.4 mmol), CsCO_3 (15.7 mg, 48.2 mmol) and PhICl_2 (13.3 mg, 48.4 mmol). None of the experiments produced the chlorinated aryl product.

3.5.5 X-Ray Structure Determination

Crystals of the complexes $\text{AuC}_6\text{F}_5(\text{IPr})$ and $\text{AuC}_6\text{F}_5\text{Cl}_2(\text{IPr})$ were grown from a mixture of dichloromethane and pentane through slow evaporation in NMR tubes. For each complex, the data crystal was selected and mounted on plastic mesh using Paratone[®] oil flash-cooled to the data collection temperature. Data were collected on a Brüker-AXS APEX CCD diffractometer with graphite-monochromated Mo- $K\alpha$ radiation ($\lambda = 0.71073 \text{ \AA}$). Unit cell parameters were obtained from 60 data frames, $0.3^\circ \omega$, from three different sections of the Ewald sphere. The systematic absences in the data and the unit cell parameters were consistent to Cc and C2/c. Refinement in the centrosymmetric space group yielded stable refinement results. The data-sets were treated with SADABS absorption corrections based on redundant multiscan data. The structure was solved using direct methods and refined with full-matrix, least-squares procedures on F^2 . All non-hydrogen atoms were refined with anisotropic displacement parameters. All hydrogen atoms were treated as idealized contributions. Scattering factors are contained in the SHELXTL 6.12 program library.

REFERENCES

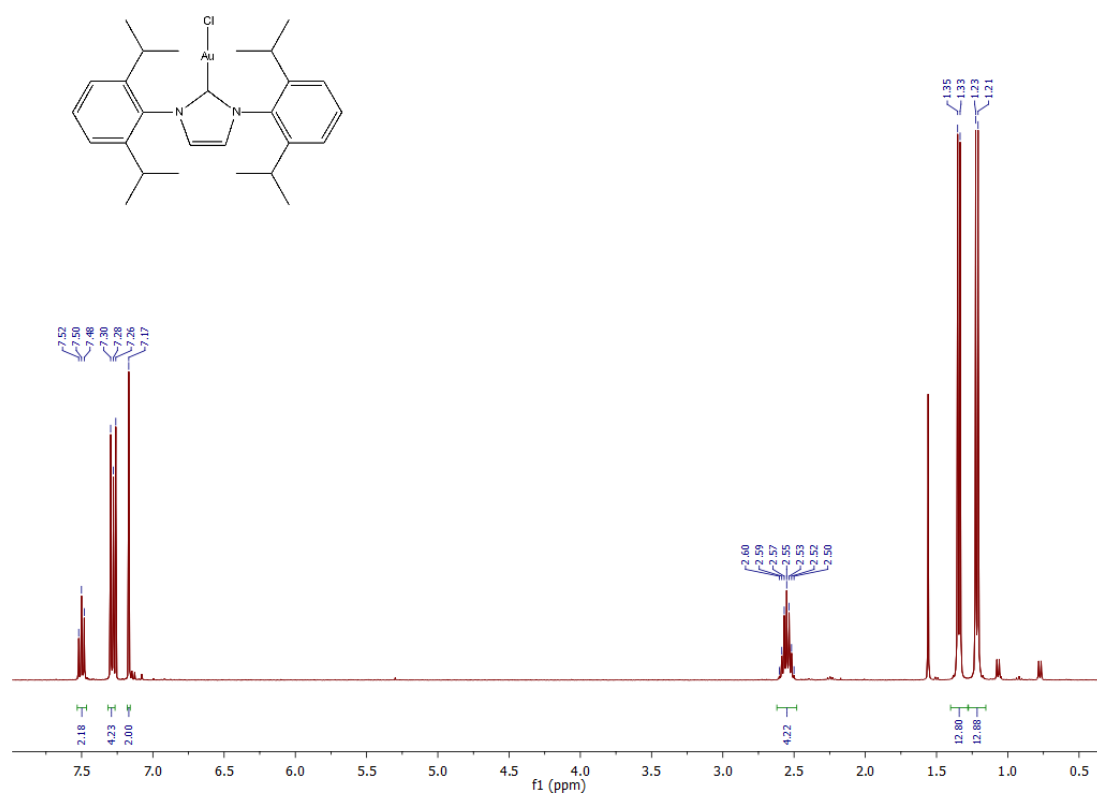
1. *Climate Change 2007: Mitigation of Climate Change*; IPCC Working Group III Fourth Assessment Report; Intergovernmental Panel on Climate Change: Geneva, 2007.
2. National Oceanic and Atmospheric Administration. Trends in Atmospheric Carbon Dioxide. http://www.esrl.noaa.gov/gmd/ccgg/trends/#mlo_full (accessed May 22, 2012).
3. Arrhenius, S. *Philosophical Magazine and Journal of Science, Series 5*. **1896**, *41*, 237–276.
4. Yagbasan, O. and Yazicigil, H. *Environ. Earth Sci.*, **2012**, *66*, 83–96.
5. Fatorić, S. and Chelleri, L. *Ocean & Coastal Management*, **2012**, *60*, 1–10.
6. Lenzen, M. and Schaeffer, R. *Climatic Change*, **2012**, *112*, 601–632.
7. Hoffert, M. I.; Caldeira, K.; Jain, A. K.; Haites, E. F.; Harvey, L. D. D.; Potter, S. D.; Schlesinger, M. E.; Schneider, S. H.; Watts, R. G.; Wigley, T. M. L.; Wuebbles, D. J. *Nature*, **1998**, *395*, 881.
8. Lewis, N. S.; Nocera, D. G. *Proc. Natl. Acad. Sci. U.S.A.*, **2006**, *103*, 15729.
9. Nocera, D.G., Cook, T., Dogutan, D., Reece, S., Surendranath, Y., Teets, T. *Chem. Rev.*, **2010**, *110*, 6474–6502.
10. Abbott, D. *Proc. IEEE*, **2010**, *98*, 42–66.
11. Barber, J. *Chem. Soc. Rev.*, **2009**, *38*, 185–196.
12. Teets, T.S. and Nocera, D.G. *Chem. Comm.*, **2011**, *47*, 9268–9274.
13. Hellot, H. ‘Histoire de l’academie royale des sciences’ **1737**, 101.
14. Klein, M.P., Yachandra, V.K., Sauer, K. *Chem. Rev.* **1996**, *96*, 2927–2950.
15. Yagi, M. and Kaneko, M. *Chem. Rev.* **2001**, *101*, 21–35.

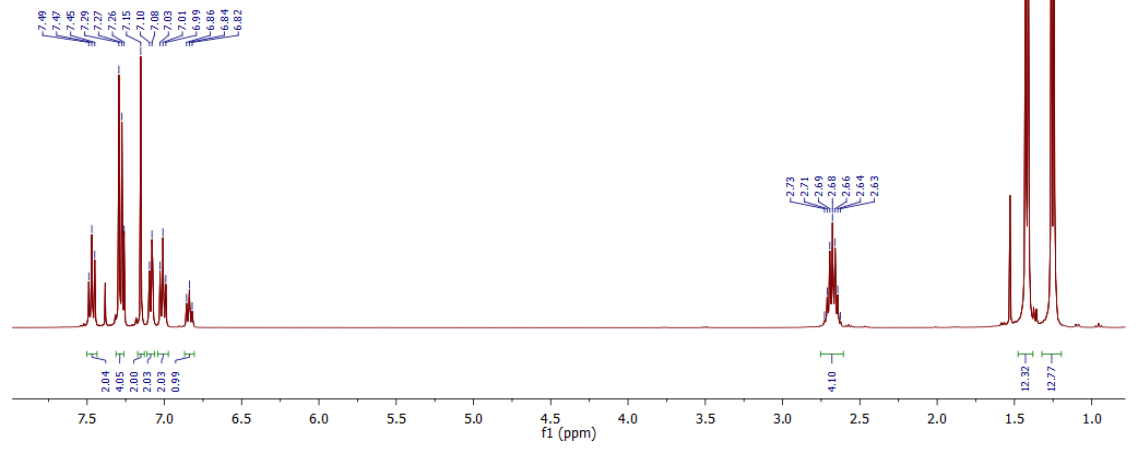
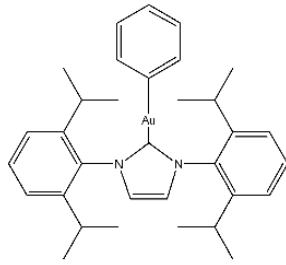
16. Meyer, T.J., Gersten, S.W., Samuels, G.J. *J. Am. Chem. Soc.*, **1982**, *104* (14), 4029–4030.
17. Meyer, T.J., Jurss, J.W., Concepcion, J.J., Butler, J.M., Omberg, K.M., Baraldo, L.M., Thompson, D.G., Lebeau, E.L., Hornstein, B., Schoonover, J.R., Jude, H., Thompson, J.D., Dattelbaum, D.M., Rocha, R.C., Templeton, J.L. *Inorg. Chem.*, **2012**, *51* (3), 1345–1358.
18. Costas, M., Fillol, J., Codolà, Z., Garcia-Bosch, I., Gómez, L., Pla, J. *Nature Chemistry*, **2011**, *3*, 807–813.
19. Nocera, D.G., Reece, S.Y., Hamel, J.A., Sung, K., Jarvi, T.D., Esswein, A.J., Pijpers, J.J.H. *Science*, **2011**, *334* (6056), 645–648.
20. Sun, L., Duan, L., Xu, Y., Zhang, P., Wang, M. *Inorg. Chem.*, **2010**, *49* (1), 209–215.
21. Hurst, J.K., Cape, J.L., Clark, A.E., Das, S., and Qin, C. *Inorg. Chem.*, **2008**, *47* (6), 1753–1764.
22. Nocera, D., Dempsey, J., Esswein, A., Manke, D., Rosenthal, J., Soper, J. *Inorg. Chem.*, **2005**, *44*, 6879–6892.
23. Nocera, D.G. and Heyduk, A. *Science*, **2001**, *293*, 5535, 1639–1641.
24. Teets, T.S. and Nocera, D.G. *J. Am. Chem. Soc.*, **2009**, *131*, 7411–7420.
25. Lee, C.H., Cook, T.R. and Nocera, D.G. *Inorg. Chem.*, **2011**, *50*, 714–716.
26. Vogler, A. and Kunkely, H. *Coord. Chem. Rev.* *219–221*, **2001**, 489–507.
27. Serafimova, I. and Hoggard, P. *Inorg. Chim. Acta*, **2002**, *338*, 105–110.
28. Wanzlick, H.W. *Angew. Chem. Int. Ed.*, **1962**, *1*, 75–80.
29. Wanzlick, H.W. and Schönherr, H.J. *Angew. Chem. Int. Ed.*, **1968**, *7*, 141–142.
30. Lappert, M., Cetinkaya, B., Dixneuf, P. *J. Chem. Soc., Dalton Trans.*, **1974**, 1827–1833.
31. Lin, I.J.B., Lin, J.C.Y., Huang, R.T.W., Lee, C.S., Bhattacharyya, A., Hwang, W.S. *Chem. Rev.*, **2009**, *109*, 3561–3598.

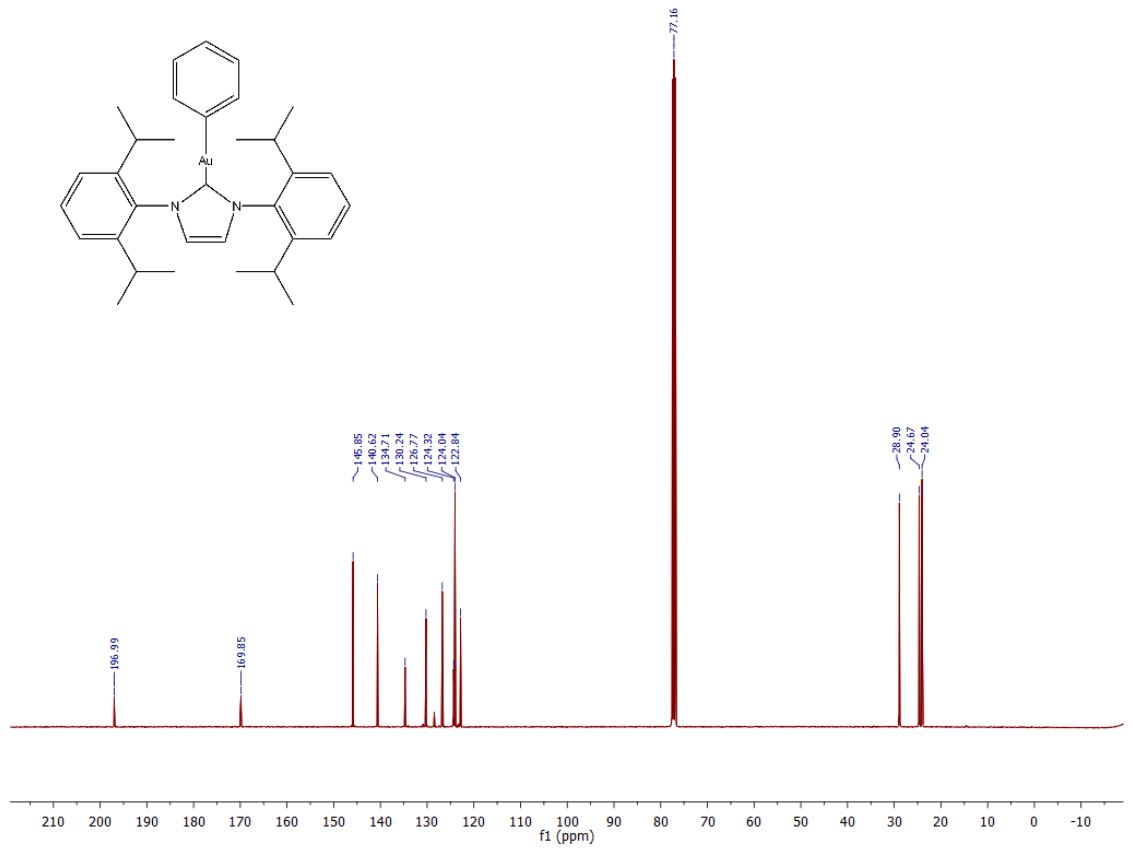
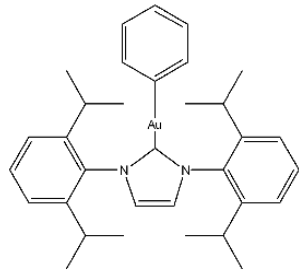
32. Limbach, M., Pažický, M., Loos, A., João Ferreira, M., Serra, D., Vinokurov, N., Rominger, F., Jäkel, C., Hashmi, A.S.K. *Organometallics*, **2010**, *29*, 4448–4458.
33. Nolan S.P., de Frémont, P., Scott, N.M., Stevens, E.D. *Organometallics*, **2005**, *24*, 2411–2418.
34. Nolan, S.P., Gaillard, S., Slawin, A.M.Z., Bonura, A.T., Stevens, E.D. *Organometallics*, **2010**, *29*, 394–402.
35. Nolan, S.P., Gaillard, S., Slawin, A.M.Z. *Chem. Comm.*, **2010**, *46*, 2742–2744.
36. Zhang, C. and Zhao, X. *Synthesis*, **2007**, *4*, 551–557.
37. Gray, T.G., Partyka, D.V., Esswein, A.J., Zeller, M., Hunter, A.D. *Organometallics*, **2007**, *26*, 3279–3282.
38. Monkowius, U., Hirtenlehner, C., Krims, C., Hölbling, J., List, M., Zabel, M., Fleck, M., Berger, R.J.F., Schoefberger, W. *Dalton Trans.*, **2011**, *40*, 9899–9910.
39. Bercaw, J., Labinger, J., Scott, V. *Organometallics*, **2010**, *29*, 4090–4096.
40. Wang, J., Mo, F., Mingtao Yan, J., Qiu, D., Li, F., Zhang, Y. *Angew. Chem. Int. Ed.*, **2010**, *49*, 2028–2032.
41. Larrosa, I., Lu, P., Boorman, T.C., Slawin, A.M.Z. *J. Am. Chem. Soc.*, **2010**, *132*, 5580–5581.
42. Kochi, J., Komiya, S., Albright, T., Hoffman, R. *J. Am. Chem. Soc.*, **1976**, *98* (23), 7255–7265.
43. Kochi, J., and Komiya, S. *J. Am. Chem. Soc.*, **1976**, *98* (24), 7599–7607.
44. Sabater, M., Corma, A., Leyva-Pérez, A. *Chem. Rev.*, **2011**, *111*, 1657–1712.
45. Toste, D. and Mankad, N. *J. Am. Chem. Soc.*, **2010**, *132*, 12859–12861.
46. Toste, D. and Mankad, N. *Chem. Sci.*, **2012**, *3*, 72–76.

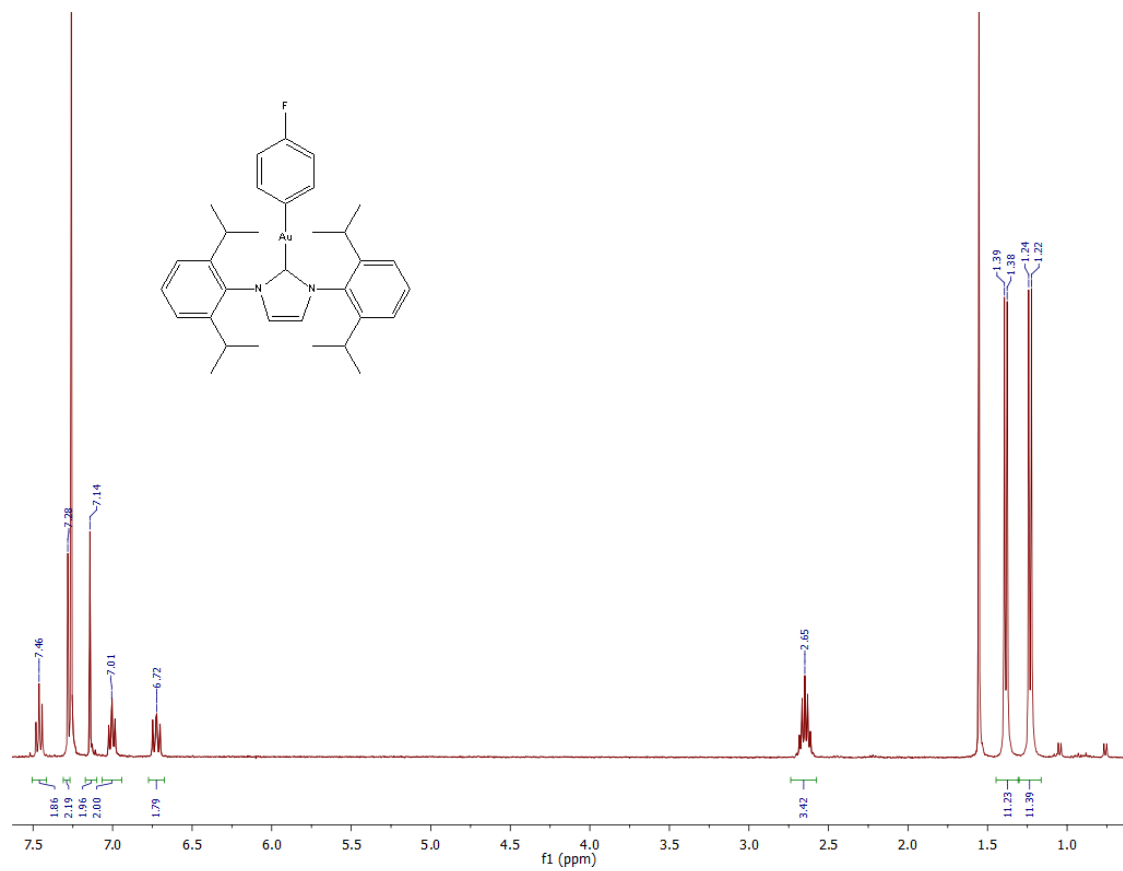
Appendix A

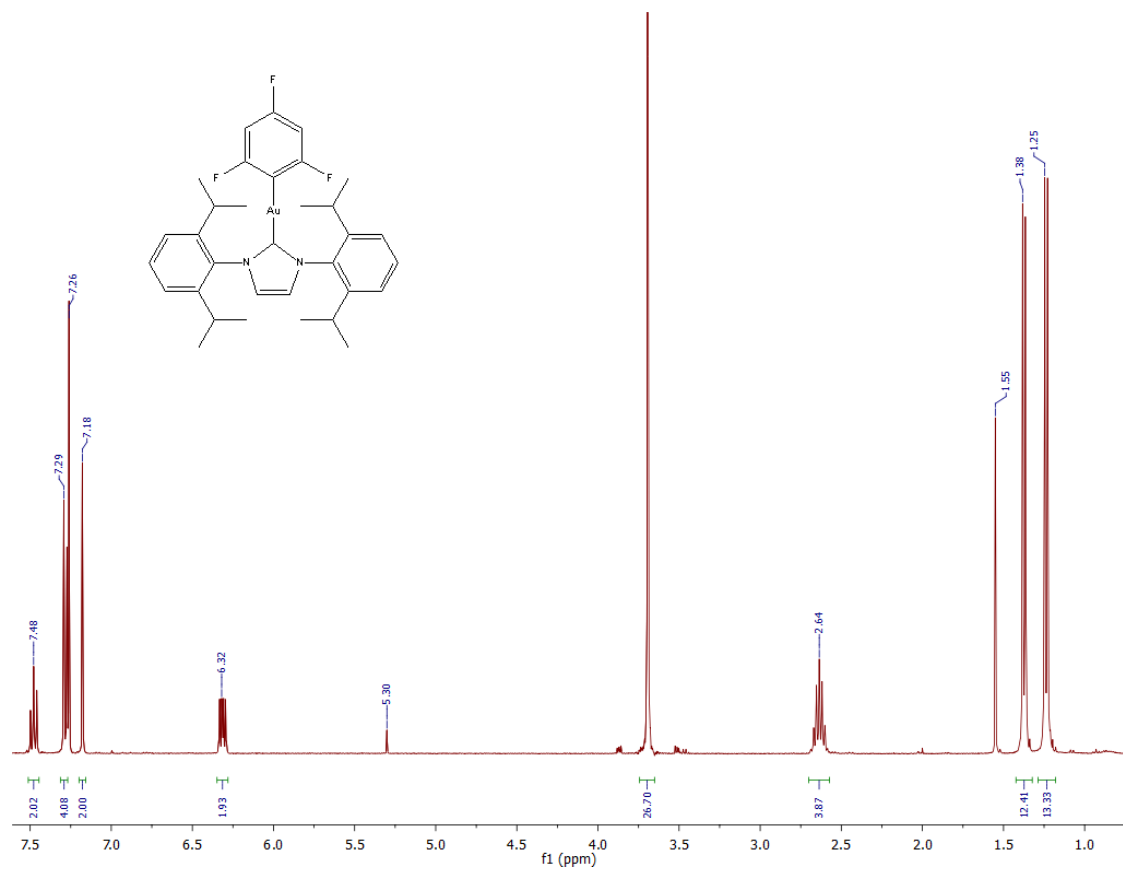
NMR Spectra. ^1H NMR spectra were recorded at 400 MHz on Bruker spectrometers and were referenced to the residual solvent peak at 7.26 ppm (CDCl_3). ^{13}C NMR spectra were recorded at 100 MHz and referenced to the residual solvent peak at 77.16 ppm (CDCl_3).

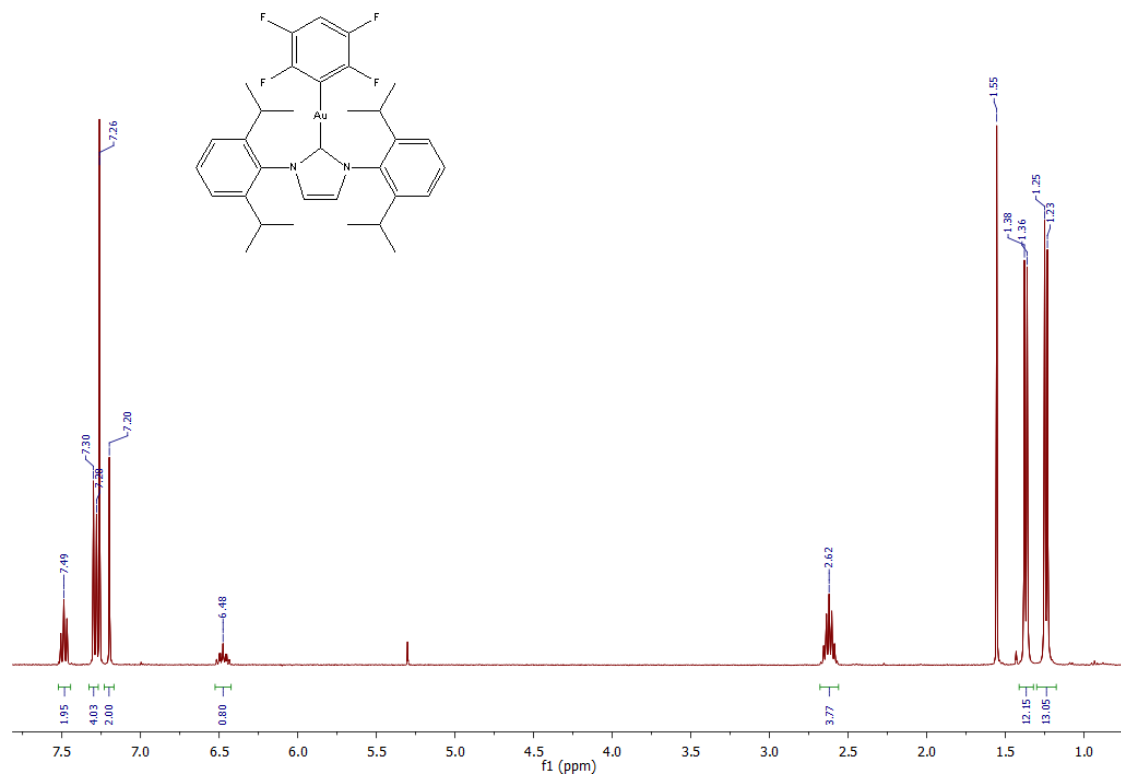


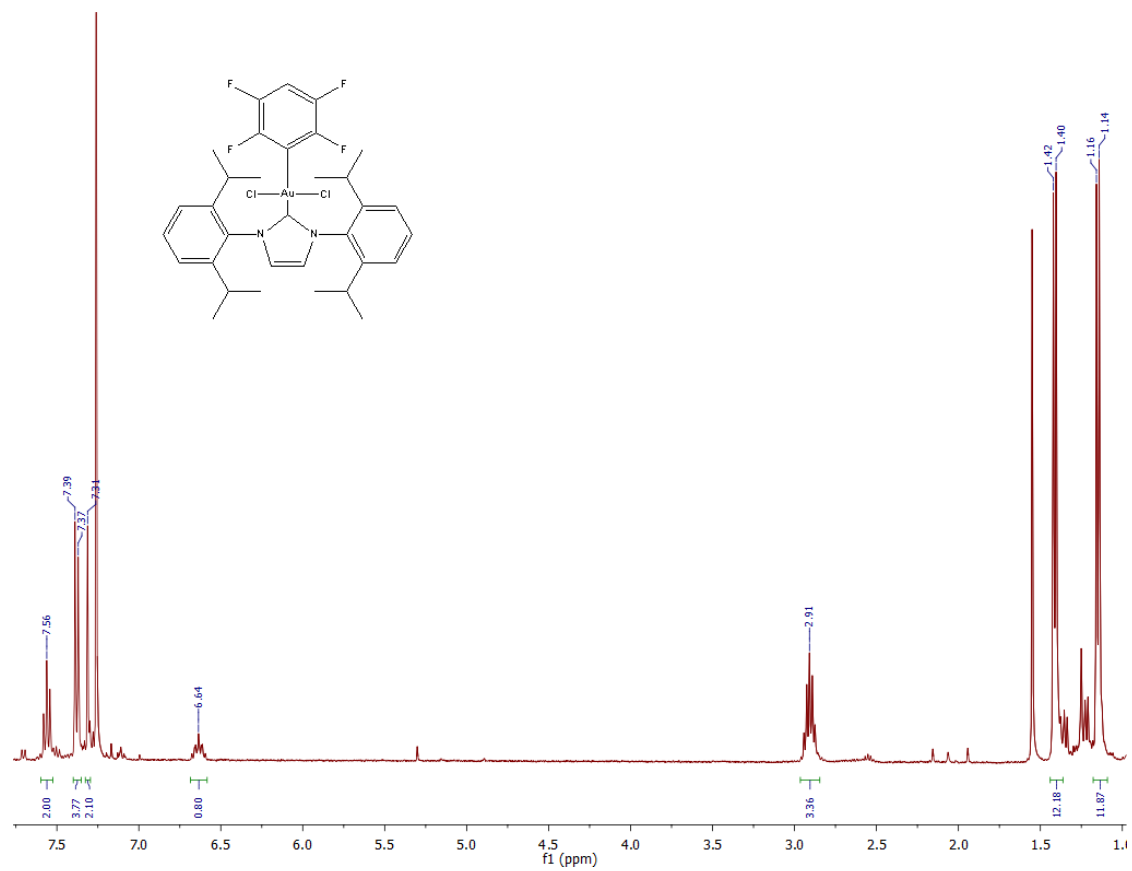


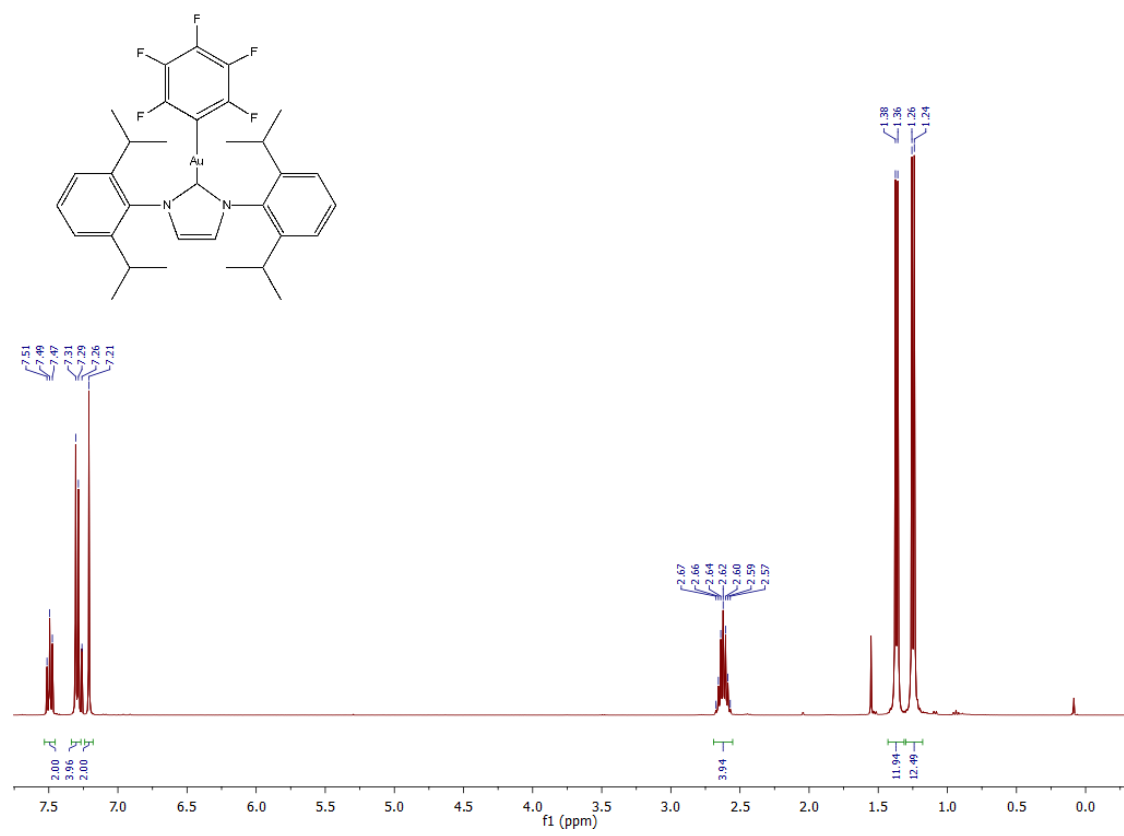


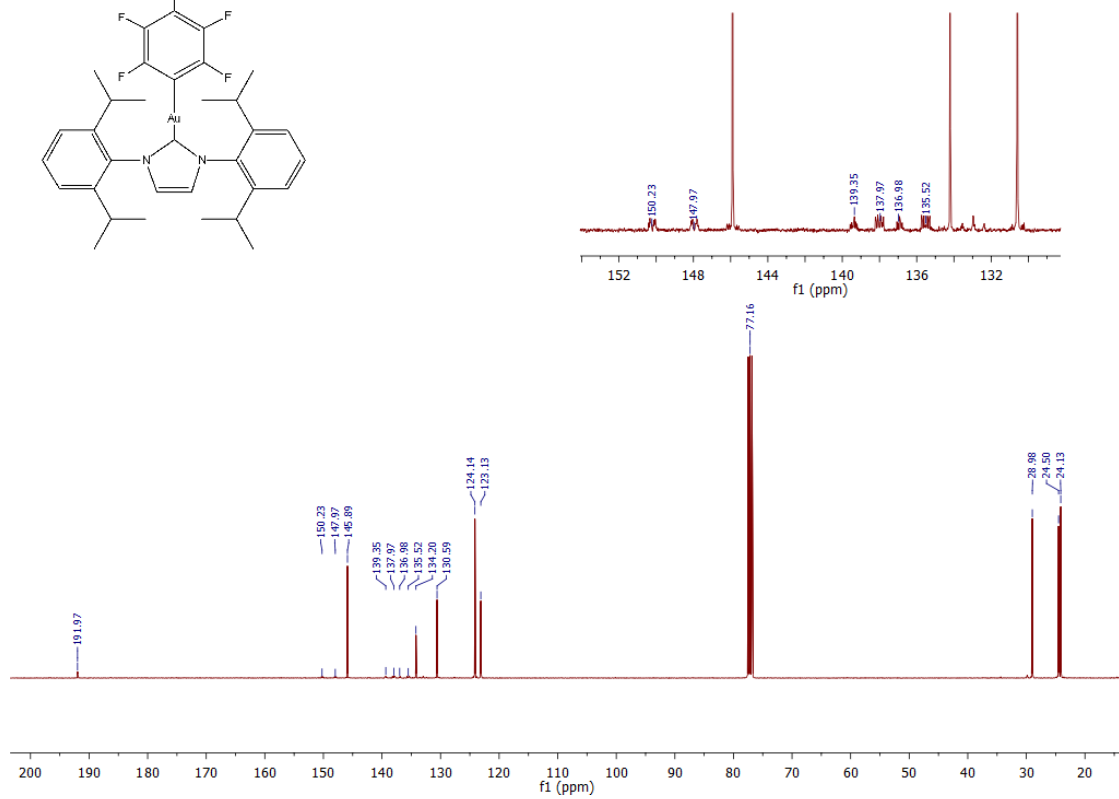
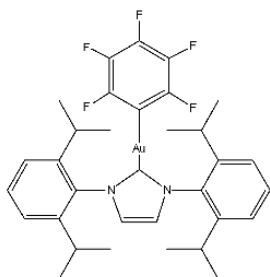


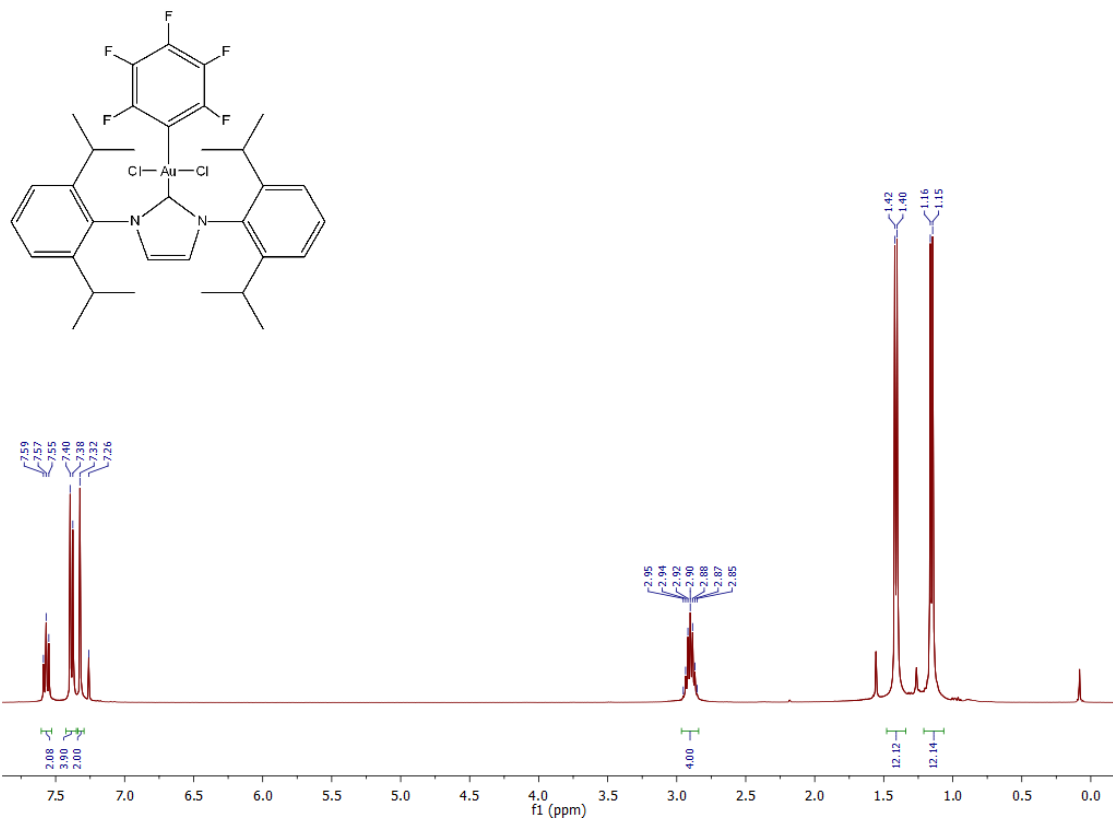


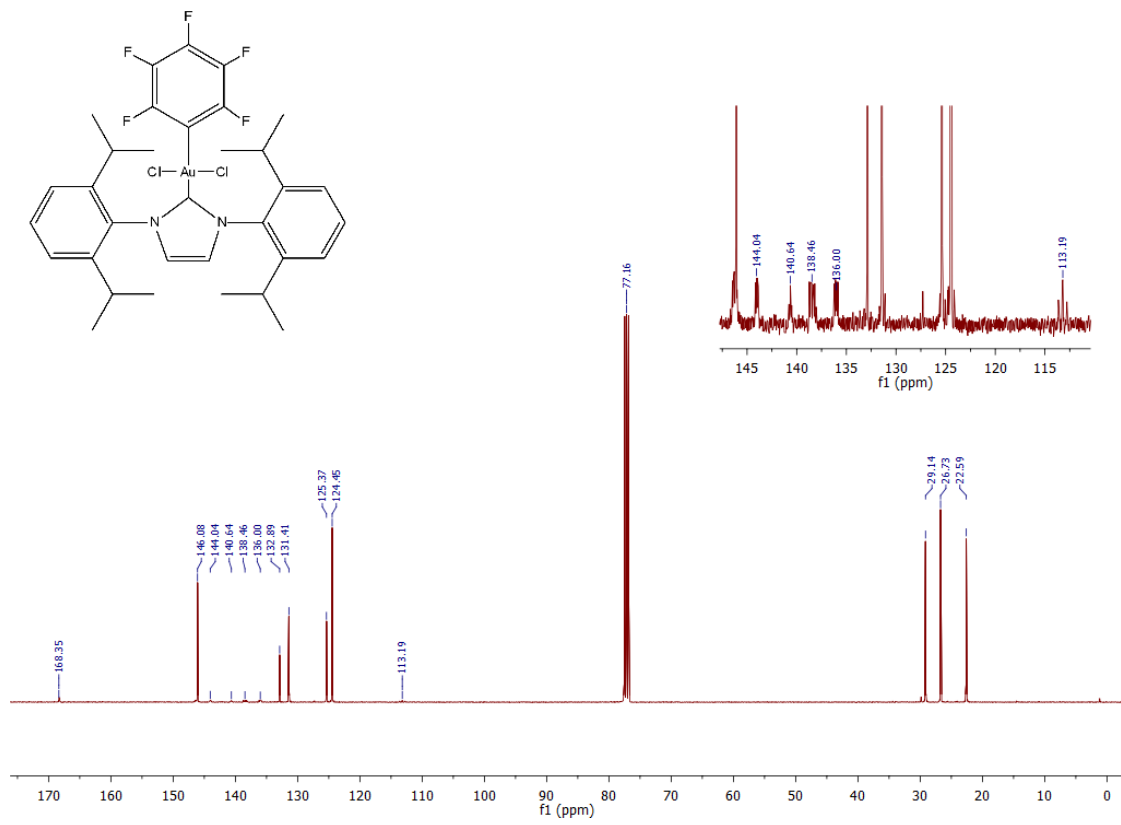


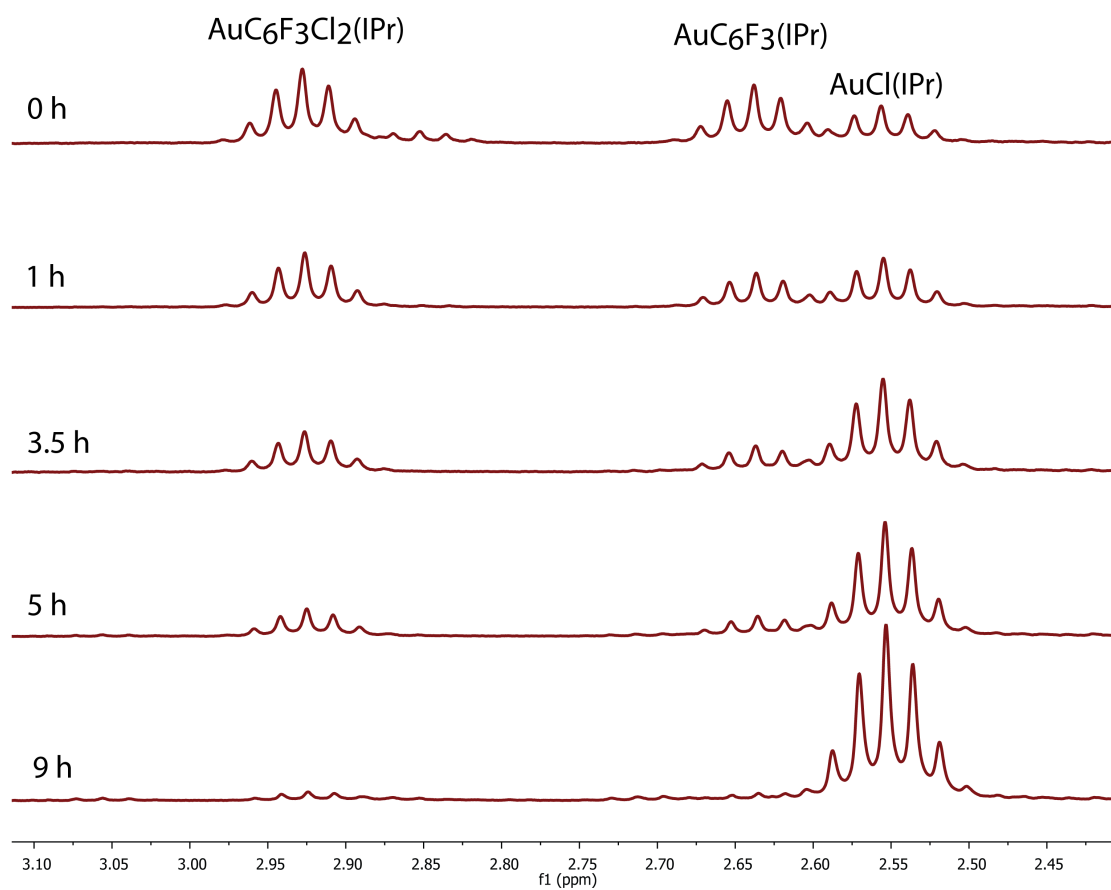




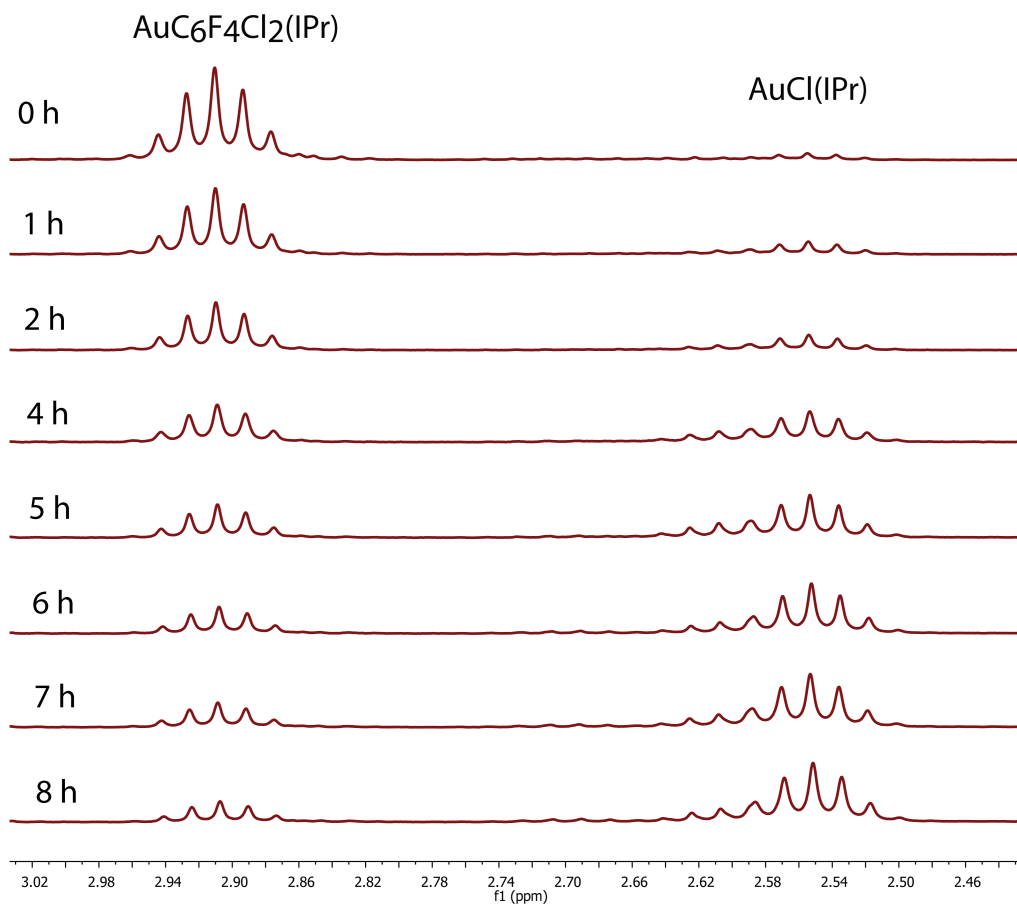








Photoreduction of $\text{AuC}_6\text{H}_2\text{F}_3(\text{IPr})$: ^1H NMR (400 MHz, CDCl_3). Internal standard: 1,4-dioxane ($\delta = 3.7$) (not shown).

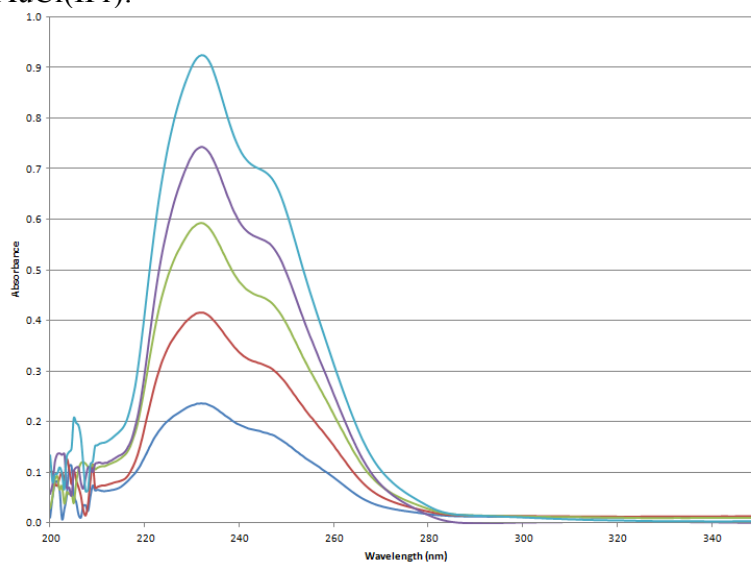


Photoreduction of $\text{AuC}_6\text{HF}_4(\text{IPr})$: ^1H NMR (400 MHz, CDCl_3). Internal standard: 1,4-dioxane ($\delta = 3.7$) (not shown).

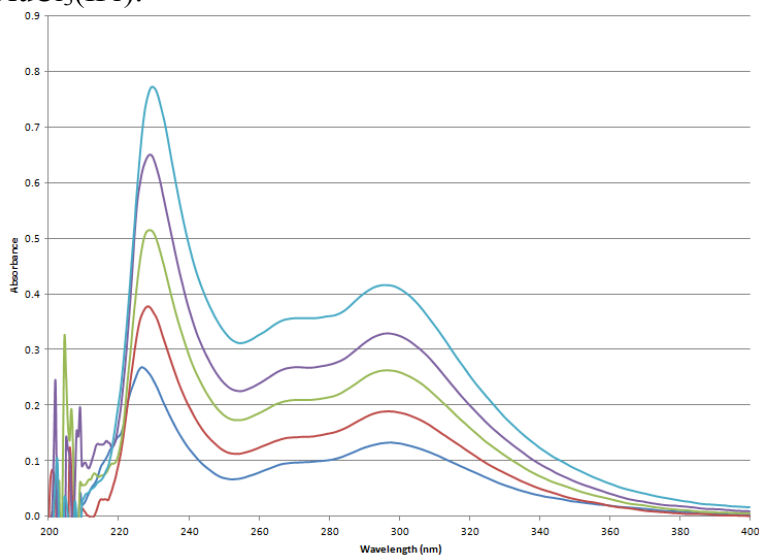
UV-Vis Spectra. Spectra were recorded on a StellarNet fiber optic UV-Vis spectrophotometer between 190 nm and 1078.5 nm with a 1.0 cm quartz cuvette.

Beer's Law Plots: solutions of gold complexes were prepared in 20, 40, 60, 80 and 100 μM concentrations, diluted from 150 μM stock solutions.

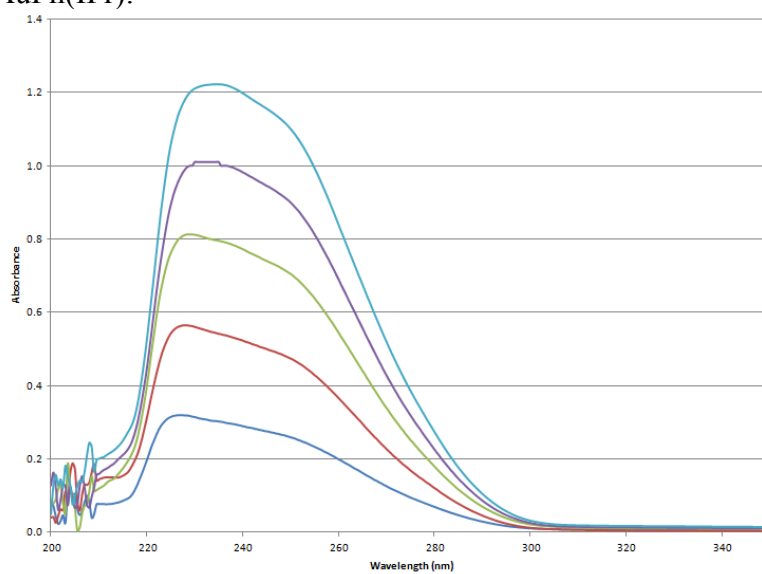
AuCl(IPr):



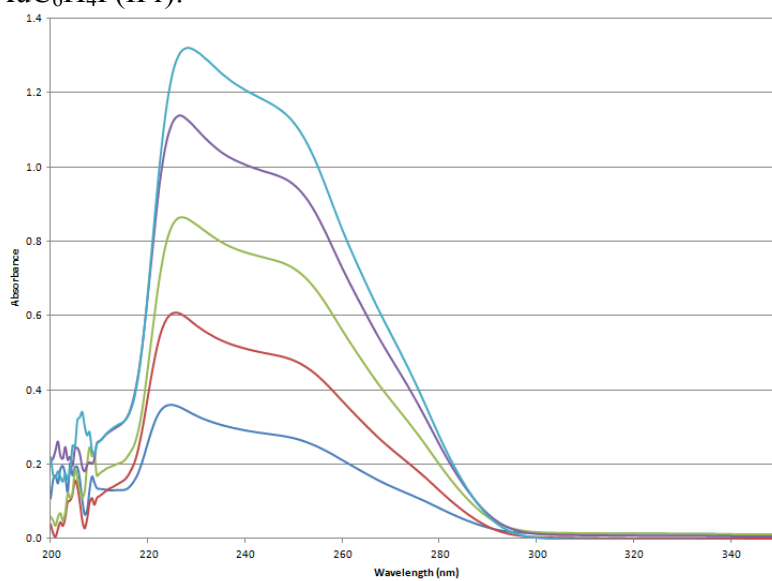
AuCl₃(IPr):



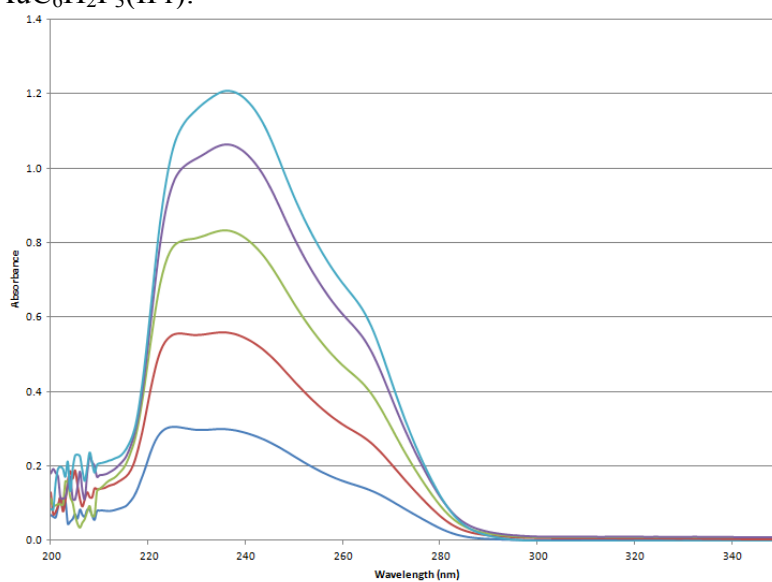
AuPh(IPr):



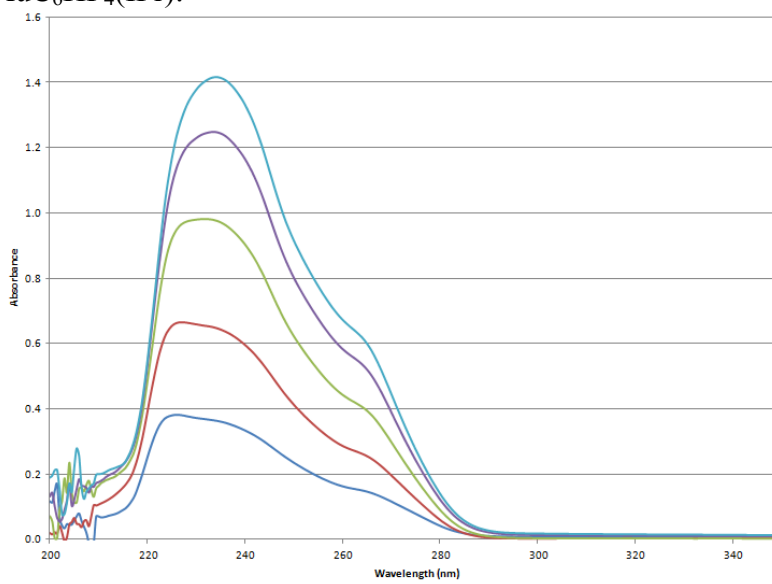
AuC₆H₄F(IPr):



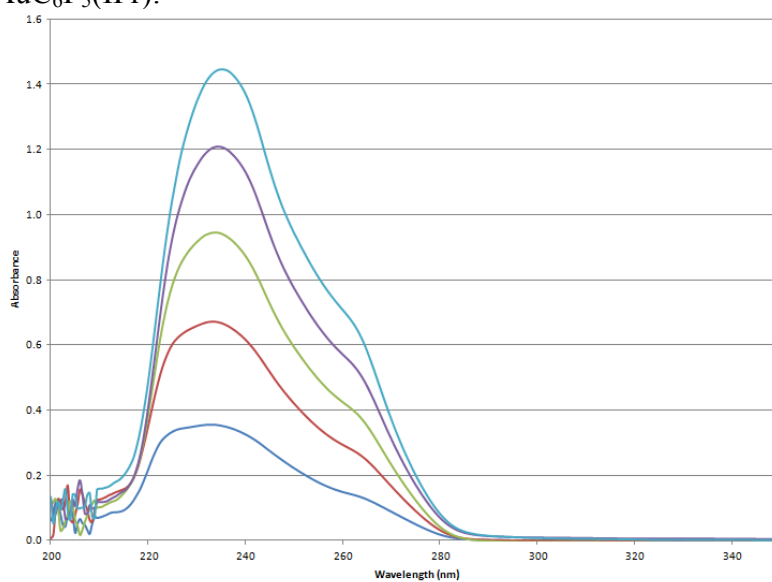
$\text{AuC}_6\text{H}_2\text{F}_3(\text{IPr})$:



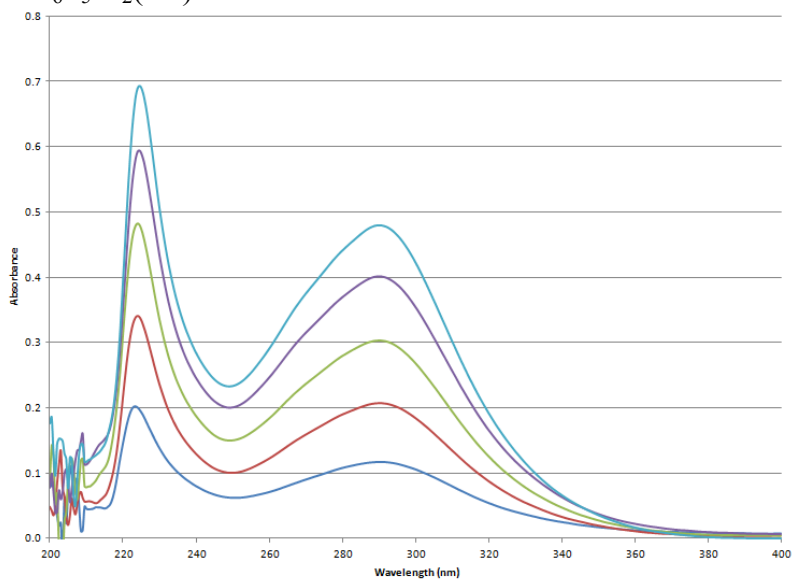
$\text{AuC}_6\text{HF}_4(\text{IPr})$:



$\text{AuC}_6\text{F}_5(\text{IPr})$:



$\text{AuC}_6\text{F}_5\text{Cl}_2(\text{IPr})$:



Crystallographic Data.

AuC₆F₅(IPr):

Table 1. Crystal data and structure refinement for AuC₆F₅(IPr).

Empirical formula	C ₃₃ H ₃₆ AuF ₅ N ₂
Formula weight	752.60
Temperature	200(2) K
Wavelength	0.71073 Å
Crystal system, space group	Monoclinic, C2/c
Unit cell dimensions	a = 10.8899(16) Å alpha = 90° b = 20.677(3) Å beta = 99.470(2)° c = 14.218(2) Å gamma = 90°
Volume	3157.7(8) Å ³
Z, Calculated density	4, 1.583 g/cm ³
Absorption coefficient	4.712 mm ⁻¹
F(000)	1488
Crystal size	0.34 x 0.31 x 0.13 mm
θ range for data collection	1.97 to 28.29°
Limiting indices	-14 ≤ h ≤ 14, -27 ≤ k ≤ 25, -18 ≤ l ≤ 18
Reflections collected / unique	19482 / 3926 [R(int) = 0.0592]
Completeness to θ = 25.00	100.0 %
Absorption correction	Semi-empirical from equivalents
Max. and min. transmission	0.5882 and 0.3013
Refinement method	Full-matrix least-squares on F ²
Data / restraints / parameters	3926 / 0 / 192
Goodness-of-fit on F ²	1.030
Final R indices [I > 2σ(I)]	R1 = 0.0307, wR2 = 0.0569
R indices (all data)	R1 = 0.0378, wR2 = 0.0596
Largest diff. peak and hole	0.892 and -0.556 e. Å ⁻³

Table 2. Atomic coordinates (× 10⁴) and equivalent isotropic displacement parameters (Å² × 10³) for AuC₆F₅(IPr). U(eq) is defined as one third of the trace of the

orthogonalized U_{ij} tensor.

	x	y	z	U(eq)
Au	0	2673(1)	2500	32(1)
F(1)	1914(2)	1622(1)	1921(2)	56(1)
F(2)	1932(3)	330(1)	1958(2)	78(1)
F(3)	0	-332(2)	2500	83(1)
N(1)	265(2)	4053(1)	3259(2)	31(1)
C(1)	0	3649(2)	2500	29(1)
C(2)	164(3)	4693(2)	2979(2)	37(1)
C(3)	1699(3)	3746(2)	4702(2)	40(1)
C(4)	1841(4)	3563(2)	5658(3)	54(1)
C(5)	821(4)	3482(2)	6114(3)	57(1)
C(6)	-364(4)	3574(2)	5636(3)	54(1)
C(7)	-570(3)	3749(2)	4679(2)	42(1)
C(8)	474(3)	3839(2)	4244(2)	33(1)
C(9)	2808(3)	3813(2)	4189(3)	47(1)
C(10)	3149(4)	3164(3)	3805(4)	78(2)
C(11)	3961(4)	4101(2)	4796(3)	66(1)
C(12)	-1883(3)	3852(2)	4147(3)	49(1)
C(13)	-2703(4)	3261(2)	4189(4)	72(1)
C(14)	-2453(4)	4453(2)	4520(4)	73(1)
C(15)	938(3)	1319(2)	2216(2)	40(1)
C(16)	973(4)	654(2)	2220(3)	49(1)
C(17)	0	323(3)	2500	54(2)
C(33)	0	1696(2)	2500	34(1)

Table 3. Bond lengths [\AA] and angles [deg] for $\text{AuC}_6\text{F}_5(\text{IPr})$.

Au-C(1)	2.018(4)
Au-C(33)	2.021(5)
F(1)-C(15)	1.358(4)
F(2)-C(16)	1.343(4)
F(3)-C(17)	1.355(6)
N(1)-C(1)	1.358(4)
N(1)-C(2)	1.381(4)
N(1)-C(8)	1.450(4)

C(1)-N(1)#1	1.358(4)
C(2)-C(2)#1	1.350(6)
C(3)-C(4)	1.394(5)
C(3)-C(8)	1.399(5)
C(3)-C(9)	1.516(5)
C(4)-C(5)	1.385(6)
C(5)-C(6)	1.369(5)
C(6)-C(7)	1.390(5)
C(7)-C(8)	1.394(5)
C(7)-C(12)	1.519(5)
C(9)-C(10)	1.517(6)
C(9)-C(11)	1.524(5)
C(12)-C(13)	1.520(6)
C(12)-C(14)	1.522(6)
C(15)-C(16)	1.375(5)
C(15)-C(33)	1.397(4)
C(16)-C(17)	1.374(5)
C(17)-C(16)#1	1.374(5)
C(33)-C(15)#1	1.397(4)

C(1)-Au-C(33)	180.0
C(1)-N(1)-C(2)	111.3(3)
C(1)-N(1)-C(8)	124.0(3)
C(2)-N(1)-C(8)	124.3(3)
N(1)-C(1)-N(1)#1	104.0(4)
N(1)-C(1)-Au	127.98(19)
N(1)#1-C(1)-Au	127.98(19)
C(2)#1-C(2)-N(1)	106.63(18)
C(4)-C(3)-C(8)	115.8(3)
C(4)-C(3)-C(9)	121.7(3)
C(8)-C(3)-C(9)	122.5(3)
C(5)-C(4)-C(3)	121.4(4)
C(6)-C(5)-C(4)	120.9(4)
C(5)-C(6)-C(7)	120.6(4)
C(6)-C(7)-C(8)	117.2(3)
C(6)-C(7)-C(12)	120.8(3)
C(8)-C(7)-C(12)	122.0(3)
C(7)-C(8)-C(3)	124.0(3)
C(7)-C(8)-N(1)	117.4(3)
C(3)-C(8)-N(1)	118.6(3)
C(3)-C(9)-C(10)	110.8(3)
C(3)-C(9)-C(11)	114.2(3)
C(10)-C(9)-C(11)	108.8(3)

C(7)-C(12)-C(13)	112.2(3)
C(7)-C(12)-C(14)	110.2(3)
C(13)-C(12)-C(14)	111.5(4)
F(1)-C(15)-C(16)	116.1(3)
F(1)-C(15)-C(33)	118.6(3)
C(16)-C(15)-C(33)	125.3(4)
F(2)-C(16)-C(17)	120.3(4)
F(2)-C(16)-C(15)	121.2(4)
C(17)-C(16)-C(15)	118.5(4)
F(3)-C(17)-C(16)#1	119.8(3)
F(3)-C(17)-C(16)	119.9(3)
C(16)#1-C(17)-C(16)	120.3(5)
C(15)-C(33)-C(15)#1	112.1(5)
C(15)-C(33)-Au	123.9(2)
C(15)#1-C(33)-Au	123.9(2)

Symmetry transformations used to generate equivalent atoms: #1 -x,y,-z+1/2

Table 4. Anisotropic displacement parameters ($\text{\AA}^2 \times 10^3$) for $\text{AuC}_6\text{F}_5(\text{IPr})$. The anisotropic displacement factor exponent takes the form:

$$-2 \pi^2 [h^2 a^{*2} U11 + \dots + 2 h k a^* b^* U12]$$

	U11	U22	U33	U23	U13	U12
Au	34(1)	30(1)	30(1)	0	3(1)	0
F(1)	48(1)	62(2)	62(1)	2(1)	19(1)	6(1)
F(2)	95(2)	61(2)	81(2)	-9(1)	18(2)	36(2)
F(3)	145(4)	28(2)	71(2)	0	3(2)	0
N(1)	29(1)	30(2)	32(1)	-2(1)	1(1)	2(1)
C(1)	27(2)	26(2)	32(2)	0	4(2)	0
C(2)	34(2)	31(2)	46(2)	-4(2)	1(2)	-2(2)
C(3)	39(2)	38(2)	40(2)	-4(2)	-1(2)	4(2)
C(4)	51(2)	60(3)	44(2)	4(2)	-10(2)	9(2)
C(5)	70(3)	71(3)	31(2)	8(2)	9(2)	11(2)
C(6)	55(2)	69(3)	39(2)	2(2)	14(2)	6(2)
C(7)	41(2)	46(2)	38(2)	-3(2)	9(2)	5(2)
C(8)	39(2)	31(2)	28(2)	-3(1)	0(1)	4(1)
C(9)	31(2)	62(3)	46(2)	8(2)	-5(2)	2(2)
C(10)	44(2)	93(4)	99(4)	-44(3)	14(2)	-2(2)

C(11)	41(2)	65(3)	88(3)	-20(3)	-1(2)	1(2)
C(12)	37(2)	66(3)	46(2)	4(2)	11(2)	5(2)
C(13)	51(3)	74(4)	90(3)	-6(3)	8(2)	-5(2)
C(14)	52(3)	74(4)	92(3)	-9(3)	7(2)	16(2)
C(15)	43(2)	40(2)	36(2)	1(2)	3(2)	3(2)
C(16)	64(3)	42(2)	39(2)	-5(2)	2(2)	16(2)
C(17)	95(5)	24(3)	39(3)	0	-6(3)	0
C(33)	31(2)	47(3)	20(2)	0	-4(2)	0

Table 5. Hydrogen coordinates ($\times 10^4$) and isotropic displacement parameters ($\text{\AA}^2 \times 10^3$) for $\text{AuC}_6\text{F}_5(\text{IPr})$.

	x	y	z	U(eq)
H(2A)	299	5061	3382	45
H(4A)	2653	3492	6003	65
H(5A)	946	3362	6768	69
H(6A)	-1052	3517	5962	64
H(9A)	2558	4106	3631	57
H(10A)	2424	2984	3387	117
H(10B)	3411	2867	4338	117
H(10C)	3832	3222	3442	117
H(11A)	3738	4507	5084	99
H(11B)	4593	4188	4395	99
H(11C)	4294	3796	5301	99
H(12A)	-1823	3931	3462	59
H(13A)	-2279	2878	3995	108
H(13B)	-3493	3322	3756	108
H(13C)	-2865	3204	4841	108
H(14A)	-3271	4535	4136	110
H(14B)	-1908	4825	4476	110
H(14C)	-2547	4386	5186	110

Table 6. Torsion angles [deg] for $\text{AuC}_6\text{F}_5(\text{IPr})$.

C(2)-N(1)-C(1)-N(1)#1	0.16(16)
C(8)-N(1)-C(1)-N(1)#1	173.0(3)
C(2)-N(1)-C(1)-Au	-179.84(16)
C(8)-N(1)-C(1)-Au	-7.0(3)
C(33)-Au-C(1)-N(1)	96(100)
C(33)-Au-C(1)-N(1)#1	-84(100)
C(1)-N(1)-C(2)-C(2)#1	-0.4(4)
C(8)-N(1)-C(2)-C(2)#1	-173.3(3)
C(8)-C(3)-C(4)-C(5)	-0.3(6)
C(9)-C(3)-C(4)-C(5)	-177.8(4)
C(3)-C(4)-C(5)-C(6)	0.7(7)
C(4)-C(5)-C(6)-C(7)	0.1(7)
C(5)-C(6)-C(7)-C(8)	-1.3(6)
C(5)-C(6)-C(7)-C(12)	-179.8(4)
C(6)-C(7)-C(8)-C(3)	1.8(5)
C(12)-C(7)-C(8)-C(3)	-179.7(4)
C(6)-C(7)-C(8)-N(1)	-177.0(3)
C(12)-C(7)-C(8)-N(1)	1.5(5)
C(4)-C(3)-C(8)-C(7)	-1.0(5)
C(9)-C(3)-C(8)-C(7)	176.5(3)
C(4)-C(3)-C(8)-N(1)	177.8(3)
C(9)-C(3)-C(8)-N(1)	-4.7(5)
C(1)-N(1)-C(8)-C(7)	-84.7(4)
C(2)-N(1)-C(8)-C(7)	87.3(4)
C(1)-N(1)-C(8)-C(3)	96.4(3)
C(2)-N(1)-C(8)-C(3)	-91.6(4)
C(4)-C(3)-C(9)-C(10)	84.9(5)
C(8)-C(3)-C(9)-C(10)	-92.5(4)
C(4)-C(3)-C(9)-C(11)	-38.3(5)
C(8)-C(3)-C(9)-C(11)	144.3(4)
C(6)-C(7)-C(12)-C(13)	-56.5(5)
C(8)-C(7)-C(12)-C(13)	125.1(4)
C(6)-C(7)-C(12)-C(14)	68.5(5)
C(8)-C(7)-C(12)-C(14)	-109.9(4)
F(1)-C(15)-C(16)-F(2)	0.9(5)
C(33)-C(15)-C(16)-F(2)	-178.1(3)
F(1)-C(15)-C(16)-C(17)	-179.2(3)
C(33)-C(15)-C(16)-C(17)	1.8(5)
F(2)-C(16)-C(17)-F(3)	-0.9(4)
C(15)-C(16)-C(17)-F(3)	179.2(2)
F(2)-C(16)-C(17)-C(16)#1	179.1(4)

C(15)-C(16)-C(17)-C(16)#1	-0.8(2)
F(1)-C(15)-C(33)-C(15)#1	-179.9(3)
C(16)-C(15)-C(33)-C(15)#1	-0.9(2)
F(1)-C(15)-C(33)-Au	0.1(3)
C(16)-C(15)-C(33)-Au	179.1(2)
C(1)-Au-C(33)-C(15)	160(100)
C(1)-Au-C(33)-C(15)#1	-20(100)

Symmetry transformations used to generate equivalent atoms:
#1 -x,y,-z+1/2

AuC₆F₅Cl₂(IPr):

Table 1. Crystal data and structure refinement for AuC₆F₅Cl₂(IPr).

Empirical formula	C ₃₃ H ₃₆ Au Cl ₂ F ₅ N ₂
Formula weight	823.50
Temperature	200(2) K
Wavelength	0.71073 Å
Crystal system, space group	Monoclinic, C2/c
Unit cell dimensions	a = 31.02(2) Å alpha = 90° b = 15.281(10) Å beta = 91.920(13)° c = 16.849(11) Å gamma = 90°
Volume	7982(9) Å ³
Z, Calculated density	8, 1.370 g/cm ³
Absorption coefficient	3.864 mm ⁻¹
F(000)	3248
Crystal size	0.18 x 0.09 x 0.05 mm
θ range for data collection	1.90 to 28.30°
Limiting indices	-41 ≤ h ≤ 41, -20 ≤ k ≤ 20, -22 ≤ l ≤ 22
Reflections collected / unique	53748 / 9898 [R(int) = 0.0988]
Completeness to θ = 25.00	99.9 %
Absorption correction	Semi-empirical from equivalents
Max. and min. transmission	0.8185 and 0.5430
Refinement method	Full-matrix least-squares on F ²
Data / restraints / parameters	9898 / 0 / 396
Goodness-of-fit on F ²	1.053
Final R indices [I > 2σ(I)]	R1 = 0.0560, wR2 = 0.1308
R indices (all data)	R1 = 0.1034, wR2 = 0.1565
Largest diff. peak and hole	1.305 and -0.463 e.Å ⁻³

Table 2. Atomic coordinates ($\times 10^4$) and equivalent isotropic displacement parameters ($\text{Å}^2 \times 10^3$) for $\text{AuC}_6\text{F}_5\text{Cl}_2(\text{IPr})$. $U(\text{eq})$ is defined as one third of the trace of the orthogonalized U_{ij} tensor.

	x	y	z	U(eq)
Au	3478(1)	3907(1)	-2792(1)	47(1)
Cl(3)	3901(1)	4870(2)	-2087(1)	59(1)
C(13)	3413(2)	4710(5)	-3773(4)	46(2)
C(21)	2641(3)	5194(6)	-3682(4)	53(2)
C(20)	2625(3)	5777(6)	-3040(5)	57(2)
C(14)	3129(3)	5467(6)	-4801(4)	59(2)
C(1)	4317(3)	3824(6)	-4310(5)	60(2)
C(5)	4424(3)	5337(6)	-3860(5)	58(2)
C(16)	2 278(3)	4734(6)	-3990(5)	55(2)
C(6)	4166(2)	4653(6)	-4159(5)	51(2)
C(15)	3541(3)	5298(6)	-4951(5)	61(2)
C(10)	4254(3)	6258(7)	-3747(5)	66(3)
C(25)	3014(3)	6286(7)	-2725(6)	74(3)
C(8)	4102(4)	2241(8)	-4344(7)	90(3)
C(7)	4044(3)	3123(7)	-4704(5)	64(2)
C(22)	2285(3)	4132(7)	-4705(5)	68(3)
C(23)	2067(3)	4563(8)	-5421(5)	82(3)
C(17)	1891(3)	4880(7)	-3617(6)	70(3)
C(3)	5005(3)	4333(9)	-3789(7)	87(3)
C(19)	2229(3)	5896(7)	-2702(5)	76(3)
C(26)	3030(4)	6321(10)	-1806(7)	133(6)
C(12)	4358(4)	6845(8)	-4464(6)	91(3)
C(18)	1867(3)	5468(9)	-2982(6)	88(4)
C(2)	4756(3)	3669(8)	-4099(6)	79(3)
C(24)	2068(3)	3235(7)	-4543(7)	88(3)
C(9)	4135(3)	3105(8)	-5595(6)	84(3)
C(4)	4852(3)	5146(8)	-3689(6)	74(3)
C(11)	4419(4)	6690(7)	-2990(6)	88(3)
N(1)	3714(2)	4840(5)	-4310(4)	50(2)
N(2)	3048(2)	5088(4)	-4076(3)	50(2)
Cl(1)	3063(1)	2898(2)	-3454(1)	70(1)
C(28)	3546(3)	3044(6)	-1866(5)	59(2)

F(5)	2859(2)	3369(4)	-1406(3)	86(2)
F(1)	4250(2)	2671(5)	-2224(4)	100(2)
F(4)	2930(3)	2188(5)	-239(4)	128(3)
F(3)	3660(3)	1267(5)	-30(4)	150(4)
C(33)	3228(3)	2901(7)	-1337(5)	65(2)
F(2)	4328(3)	1520(6)	-1033(5)	146(3)
C(32)	3246(4)	2312(8)	-735(6)	84(3)
C(29)	3908(4)	2560(7)	-1753(6)	71(3)
C(31)	3611(6)	1865(8)	-629(7)	103(5)
C(30)	3950(5)	1979(8)	-1134(8)	100(4)
C(27)	3010(4)	7181(8)	-3084(10)	133(6)

Table 3. Bond lengths [Å] and angles [deg] for AuC₆F₅Cl₂(IPr).

Au-C(28)	2.049(8)
Au-C(13)	2.063(7)
Au-Cl(1)	2.278(2)
Au-Cl(3)	2.278(2)
C(13)-N(1)	1.337(9)
C(13)-N(2)	1.355(9)
C(21)-C(20)	1.403(11)
C(21)-C(16)	1.411(11)
C(21)-N(2)	1.457(10)
C(20)-C(19)	1.384(13)
C(20)-C(25)	1.517(13)
C(14)-C(15)	1.333(11)
C(14)-N(2)	1.382(9)
C(1)-C(6)	1.378(12)
C(1)-C(2)	1.414(12)
C(1)-C(7)	1.506(12)
C(5)-C(4)	1.381(12)
C(5)-C(6)	1.401(12)
C(5)-C(10)	1.516(13)
C(16)-C(17)	1.391(12)
C(16)-C(22)	1.518(12)
C(6)-N(1)	1.442(9)
C(15)-N(1)	1.382(9)
C(10)-C(11)	1.511(13)
C(10)-C(12)	1.547(13)
C(25)-C(27)	1.496(15)

C(25)-C(26)	1.548(15)
C(8)-C(7)	1.488(14)
C(7)-C(9)	1.537(12)
C(22)-C(23)	1.514(12)
C(22)-C(24)	1.555(14)
C(17)-C(18)	1.402(14)
C(3)-C(4)	1.342(14)
C(3)-C(2)	1.369(15)
C(19)-C(18)	1.368(14)
C(28)-C(29)	1.354(13)
C(28)-C(33)	1.369(12)
F(5)-C(33)	1.351(11)
F(1)-C(29)	1.355(12)
F(4)-C(32)	1.321(13)
F(3)-C(31)	1.366(12)
C(33)-C(32)	1.356(13)
F(2)-C(30)	1.371(14)
C(32)-C(31)	1.331(18)
C(29)-C(30)	1.373(15)
C(31)-C(30)	1.385(18)
C(28)-Au-C(13)	176.3(3)
C(28)-Au-Cl(1)	88.8(2)
C(13)-Au-Cl(1)	88.4(2)
C(28)-Au-Cl(3)	88.6(2)
C(13)-Au-Cl(3)	94.2(2)
Cl(1)-Au-Cl(3)	177.36(8)
N(1)-C(13)-N(2)	106.0(6)
N(1)-C(13)-Au	125.3(5)
N(2)-C(13)-Au	127.9(5)
C(20)-C(21)-C(16)	123.5(8)
C(20)-C(21)-N(2)	118.4(8)
C(16)-C(21)-N(2)	118.1(7)
C(19)-C(20)-C(21)	117.1(8)
C(19)-C(20)-C(25)	119.7(8)
C(21)-C(20)-C(25)	123.2(8)
C(15)-C(14)-N(2)	106.8(7)
C(6)-C(1)-C(2)	116.0(9)
C(6)-C(1)-C(7)	122.9(7)
C(2)-C(1)-C(7)	121.0(9)
C(4)-C(5)-C(6)	116.9(9)
C(4)-C(5)-C(10)	120.4(9)
C(6)-C(5)-C(10)	122.7(8)

C(17)-C(16)-C(21)	116.4(8)
C(17)-C(16)-C(22)	119.5(8)
C(21)-C(16)-C(22)	124.1(8)
C(1)-C(6)-C(5)	123.9(8)
C(1)-C(6)-N(1)	119.0(7)
C(5)-C(6)-N(1)	117.1(8)
C(14)-C(15)-N(1)	107.5(7)
C(11)-C(10)-C(5)	113.7(8)
C(11)-C(10)-C(12)	109.4(8)
C(5)-C(10)-C(12)	111.0(8)
C(27)-C(25)-C(20)	109.3(8)
C(27)-C(25)-C(26)	111.8(10)
C(20)-C(25)-C(26)	111.5(10)
C(8)-C(7)-C(1)	113.9(8)
C(8)-C(7)-C(9)	110.9(9)
C(1)-C(7)-C(9)	108.9(8)
C(23)-C(22)-C(16)	110.5(8)
C(23)-C(22)-C(24)	109.8(8)
C(16)-C(22)-C(24)	112.1(8)
C(16)-C(17)-C(18)	121.0(9)
C(4)-C(3)-C(2)	122.6(10)
C(18)-C(19)-C(20)	121.6(9)
C(19)-C(18)-C(17)	120.5(9)
C(3)-C(2)-C(1)	119.8(10)
C(3)-C(4)-C(5)	120.7(10)
C(13)-N(1)-C(15)	109.9(6)
C(13)-N(1)-C(6)	123.3(6)
C(15)-N(1)-C(6)	126.1(7)
C(13)-N(2)-C(14)	109.7(7)
C(13)-N(2)-C(21)	127.0(6)
C(14)-N(2)-C(21)	122.9(6)
C(29)-C(28)-C(33)	115.7(9)
C(29)-C(28)-Au	121.5(7)
C(33)-C(28)-Au	122.8(7)
F(5)-C(33)-C(32)	115.4(10)
F(5)-C(33)-C(28)	119.1(8)
C(32)-C(33)-C(28)	125.5(11)
F(4)-C(32)-C(31)	119.2(12)
F(4)-C(32)-C(33)	123.8(13)
C(31)-C(32)-C(33)	117.0(12)
F(1)-C(29)-C(28)	120.7(9)
F(1)-C(29)-C(30)	118.1(10)
C(28)-C(29)-C(30)	121.1(11)

C(32)-C(31)-F(3)	121.0(15)
C(32)-C(31)-C(30)	120.9(11)
F(3)-C(31)-C(30)	118.1(16)
C(29)-C(30)-F(2)	118.8(14)
C(29)-C(30)-C(31)	119.6(12)
F(2)-C(30)-C(31)	121.5(13)

Symmetry transformations used to generate equivalent atoms:

Table 4. Anisotropic displacement parameters ($\text{\AA}^2 \times 10^3$) for $\text{AuC}_6\text{F}_5\text{Cl}_2(\text{IPr})$. The anisotropic displacement factor exponent takes the form:

$$-2 \pi^2 [h^2 a^{*2} U11 + \dots + 2 h k a^* b^* U12]$$

	U11	U22	U33	U23	U13	U12
Au	43(1)	64(1)	33(1)	2(1)	-7(1)	1(1)
Cl(3)	56(1)	77(2)	44(1)	-3(1)	-16(1)	-5(1)
C(13)	38(4)	63(5)	36(4)	-1(3)	-6(3)	-4(4)
C(21)	51(5)	70(6)	37(4)	3(4)	-2(3)	19(4)
C(20)	60(5)	71(6)	40(4)	-4(4)	-12(4)	22(4)
C(14)	57(5)	84(6)	34(4)	16(4)	-11(4)	3(5)
C(1)	40(4)	84(7)	55(5)	-4(5)	-7(4)	-1(4)
C(5)	42(4)	83(7)	50(5)	5(4)	1(4)	0(4)
C(16)	49(5)	72(6)	44(4)	2(4)	-5(4)	3(4)
C(6)	37(4)	73(6)	44(4)	4(4)	-6(3)	-3(4)
C(15)	50(5)	98(7)	35(4)	18(4)	-5(3)	-5(5)
C(10)	54(5)	88(7)	56(5)	-1(5)	-11(4)	-8(5)
C(25)	72(6)	80(7)	70(6)	-29(5)	-31(5)	18(5)
C(8)	77(7)	100(9)	91(8)	-8(7)	-16(6)	-3(6)
C(7)	48(5)	84(7)	59(5)	-2(5)	-6(4)	10(5)
C(22)	54(5)	91(7)	58(5)	-13(5)	-13(4)	6(5)
C(23)	74(7)	124(9)	46(5)	-15(6)	-15(5)	17(6)
C(17)	50(5)	100(8)	60(6)	6(5)	1(4)	0(5)
C(3)	48(6)	121(10)	92(8)	-21(7)	-21(5)	15(6)
C(19)	74(7)	105(8)	48(5)	-18(5)	-10(5)	33(6)
C(26)	85(9)	216(16)	94(9)	-86(10)	-37(7)	44(9)
C(12)	89(8)	110(9)	74(7)	17(7)	-9(6)	-6(7)
C(18)	63(6)	147(11)	53(6)	9(7)	12(5)	29(7)
C(2)	57(6)	100(8)	80(7)	-8(6)	-10(5)	11(6)

C(24)	66(6)	91(8)	105(9)	-22(7)	-17(6)	-23(6)
C(9)	64(6)	121(10)	66(6)	-18(6)	-7(5)	1(6)
C(4)	53(6)	95(8)	73(6)	-9(6)	-9(5)	-8(5)
C(11)	108(9)	82(8)	73(7)	-8(6)	-11(6)	-15(7)
N(1)	38(3)	72(5)	38(3)	10(3)	-4(3)	1(3)
N(2)	45(4)	70(5)	34(3)	-1(3)	-6(3)	2(3)
Cl(1)	79(2)	78(2)	50(1)	6(1)	-19(1)	-22(1)
C(28)	64(6)	68(6)	44(4)	8(4)	-17(4)	-6(5)
F(5)	71(4)	123(5)	63(3)	-4(3)	5(3)	-16(4)
F(1)	83(4)	131(6)	85(4)	14(4)	-8(4)	41(4)
F(4)	154(7)	162(7)	67(4)	24(4)	14(4)	-67(6)
F(3)	237(10)	121(6)	87(5)	52(4)	-64(6)	-51(6)
C(33)	69(6)	82(7)	42(5)	4(4)	-14(4)	-15(5)
F(2)	169(8)	141(7)	124(6)	30(5)	-51(6)	57(6)
C(32)	110(9)	87(8)	53(6)	12(6)	-19(6)	-27(7)
C(29)	81(7)	75(7)	55(5)	8(5)	-14(5)	11(6)
C(31)	169(14)	82(9)	56(7)	26(6)	-36(8)	-46(9)
C(30)	126(11)	80(8)	91(9)	-3(7)	-52(8)	24(8)
C(27)	99(10)	68(8)	227(18)	3(10)	-60(11)	-6(7)

Table 5. Hydrogen coordinates ($\times 10^4$) and isotropic displacement parameters ($\text{\AA}^2 \times 10^3$) for $\text{AuC}_6\text{F}_5\text{Cl}_2(\text{IPr})$.

	x	y	z	U(eq)
H(14A)	2930	5785	-5130	71
H(15A)	3687	5463	-5413	73
H(10A)	3933	6218	-3723	80
H(25A)	3279	5978	-2898	89
H(8A)	4045	2269	-3776	134
H(8B)	4399	2043	-4413	134
H(8C)	3902	1828	-4605	134
H(7A)	3735	3293	-4650	76
H(22A)	2593	4021	-4831	81
H(23A)	2215	5111	-5540	122
H(23B)	1765	4687	-5307	122
H(23C)	2078	4169	-5879	122
H(17A)	1639	4576	-3796	83

H(3A)	5297	4215	-3639	105
H(19A)	2208	6284	-2264	91
H(26A)	3072	5729	-1593	199
H(26B)	2758	6561	-1620	199
H(26C)	3270	6694	-1623	199
H(12A)	4227	7423	-4396	137
H(12B)	4241	6577	-4954	137
H(12C)	4671	6909	-4497	137
H(18A)	1599	5571	-2744	105
H(2A)	4877	3105	-4171	95
H(24A)	2101	2850	-5002	131
H(24B)	1761	3325	-4452	131
H(24C)	2206	2966	-4072	131
H(9A)	960	2648	-5856	126
H(9B)	4442	2980	-5665	126
H(9C)	4063	3674	-5831	126
H(4A)	5041	5595	-3499	89
H(11A)	4397	6279	-2546	132
H(11B)	4245	7211	-2886	132
H(11C)	4721	6860	-3044	132
H(27A)	3056	7137	-3655	199
H(27B)	3240	7535	-2833	199
H(27C)	2730	7460	-2998	199

Table 6. Torsion angles [deg] for AuC₆F₅Cl₂(IPr).

C(28)-Au-C(13)-N(1)	-65(5)
Cl(1)-Au-C(13)-N(1)	-103.0(7)
Cl(3)-Au-C(13)-N(1)	76.5(7)
C(28)-Au-C(13)-N(2)	104(5)
Cl(1)-Au-C(13)-N(2)	65.4(7)
Cl(3)-Au-C(13)-N(2)	-115.1(7)
C(16)-C(21)-C(20)-C(19)	0.0(13)
N(2)-C(21)-C(20)-C(19)	177.0(8)
C(16)-C(21)-C(20)-C(25)	-178.5(8)
N(2)-C(21)-C(20)-C(25)	-1.5(12)
C(20)-C(21)-C(16)-C(17)	-0.5(13)
N(2)-C(21)-C(16)-C(17)	-177.5(7)
C(20)-C(21)-C(16)-C(22)	177.3(8)

N(2)-C(21)-C(16)-C(22)	0.3(12)
C(2)-C(1)-C(6)-C(5)	3.7(13)
C(7)-C(1)-C(6)-C(5)	-173.9(8)
C(2)-C(1)-C(6)-N(1)	-175.8(8)
C(7)-C(1)-C(6)-N(1)	6.5(13)
C(4)-C(5)-C(6)-C(1)	-1.9(13)
C(10)-C(5)-C(6)-C(1)	176.2(8)
C(4)-C(5)-C(6)-N(1)	177.6(8)
C(10)-C(5)-C(6)-N(1)	-4.2(12)
N(2)-C(14)-C(15)-N(1)	-1.7(10)
C(4)-C(5)-C(10)-C(11)	-42.4(12)
C(6)-C(5)-C(10)-C(11)	139.5(9)
C(4)-C(5)-C(10)-C(12)	81.5(10)
C(6)-C(5)-C(10)-C(12)	-96.6(10)
C(19)-C(20)-C(25)-C(27)	-82.0(12)
C(21)-C(20)-C(25)-C(27)	96.4(12)
C(19)-C(20)-C(25)-C(26)	42.2(12)
C(21)-C(20)-C(25)-C(26)	-139.4(9)
C(6)-C(1)-C(7)-C(8)	-138.7(9)
C(2)-C(1)-C(7)-C(8)	43.7(13)
C(6)-C(1)-C(7)-C(9)	96.9(10)
C(2)-C(1)-C(7)-C(9)	-80.6(11)
C(17)-C(16)-C(22)-C(23)	71.9(11)
C(21)-C(16)-C(22)-C(23)	-105.7(10)
C(17)-C(16)-C(22)-C(24)	-50.9(11)
C(21)-C(16)-C(22)-C(24)	131.4(9)
C(21)-C(16)-C(17)-C(18)	1.3(14)
C(22)-C(16)-C(17)-C(18)	-176.6(9)
C(21)-C(20)-C(19)-C(18)	-0.3(15)
C(25)-C(20)-C(19)-C(18)	178.2(10)
C(20)-C(19)-C(18)-C(17)	1.2(17)
C(16)-C(17)-C(18)-C(19)	-1.7(16)
C(4)-C(3)-C(2)-C(1)	-1.4(18)
C(6)-C(1)-C(2)-C(3)	-2.0(15)
C(7)-C(1)-C(2)-C(3)	175.7(10)
C(2)-C(3)-C(4)-C(5)	3.4(18)
C(6)-C(5)-C(4)-C(3)	-1.7(14)
C(10)-C(5)-C(4)-C(3)	-179.9(10)
N(2)-C(13)-N(1)-C(15)	-0.2(9)
Au-C(13)-N(1)-C(15)	170.3(6)
N(2)-C(13)-N(1)-C(6)	170.3(7)
Au-C(13)-N(1)-C(6)	-19.2(11)
C(14)-C(15)-N(1)-C(13)	1.2(10)

C(14)-C(15)-N(1)-C(6)	-168.9(8)
C(1)-C(6)-N(1)-C(13)	87.8(10)
C(5)-C(6)-N(1)-C(13)	-91.8(10)
C(1)-C(6)-N(1)-C(15)	-103.4(10)
C(5)-C(6)-N(1)-C(15)	77.1(11)
N(1)-C(13)-N(2)-C(14)	-0.9(9)
Au-C(13)-N(2)-C(14)	-171.1(6)
N(1)-C(13)-N(2)-C(21)	-173.8(7)
Au-C(13)-N(2)-C(21)	16.1(12)
C(15)-C(14)-N(2)-C(13)	1.6(10)
C(15)-C(14)-N(2)-C(21)	174.9(8)
C(20)-C(21)-N(2)-C(13)	68.7(11)
C(16)-C(21)-N(2)-C(13)	-114.1(9)
C(20)-C(21)-N(2)-C(14)	-103.3(9)
C(16)-C(21)-N(2)-C(14)	73.9(11)
C(13)-Au-C(28)-C(29)	63(5)
Cl(1)-Au-C(28)-C(29)	101.1(8)
Cl(3)-Au-C(28)-C(29)	-78.5(8)
C(13)-Au-C(28)-C(33)	-116(5)
Cl(1)-Au-C(28)-C(33)	-77.3(7)
Cl(3)-Au-C(28)-C(33)	103.1(7)
C(29)-C(28)-C(33)-F(5)	179.1(8)
Au-C(28)-C(33)-F(5)	-2.4(12)
C(29)-C(28)-C(33)-C(32)	-1.6(15)
Au-C(28)-C(33)-C(32)	176.9(8)
F(5)-C(33)-C(32)-F(4)	0.0(15)
C(28)-C(33)-C(32)-F(4)	-179.3(9)
F(5)-C(33)-C(32)-C(31)	-177.4(9)
C(28)-C(33)-C(32)-C(31)	3.3(16)
C(33)-C(28)-C(29)-F(1)	-177.5(9)
Au-C(28)-C(29)-F(1)	3.9(13)
C(33)-C(28)-C(29)-C(30)	-1.0(15)
Au-C(28)-C(29)-C(30)	-179.6(8)
F(4)-C(32)-C(31)-F(3)	1.6(17)
C(33)-C(32)-C(31)-F(3)	179.1(9)
F(4)-C(32)-C(31)-C(30)	-179.8(10)
C(33)-C(32)-C(31)-C(30)	-2.3(17)
F(1)-C(29)-C(30)-F(2)	-1.8(16)
C(28)-C(29)-C(30)-F(2)	-178.4(10)
F(1)-C(29)-C(30)-C(31)	178.4(10)
C(28)-C(29)-C(30)-C(31)	1.9(17)
C(32)-C(31)-C(30)-C(29)	-0.1(19)
F(3)-C(31)-C(30)-C(29)	178.5(9)

C(32)-C(31)-C(30)-F(2)	-179.8(11)
F(3)-C(31)-C(30)-F(2)	-1.2(18)

Symmetry transformations used to generate equivalent atoms: